Autophagy

Autophagy

ISSN: 1554-8627 (Print) 1554-8635 (Online) Journal homepage: www.tandfonline.com/journals/kaup20

Mitophagy-mediated S1P facilitates muscle adaptive responses to endurance exercise through SPHK1-S1PR1/S1PR2 in slow-twitch myofibers

Minghong Leng, Fenghe Yang, Junhui Zhao, Yufei Xiong, Yiqing Zhou, Mingyang Zhao, Shi Jia, Limei Liu, Qiaoxia Zheng, Lebin Gan, Jingjing Ye & Ming Zheng

To cite this article: Minghong Leng, Fenghe Yang, Junhui Zhao, Yufei Xiong, Yiqing Zhou, Mingyang Zhao, Shi Jia, Limei Liu, Qiaoxia Zheng, Lebin Gan, Jingjing Ye & Ming Zheng (10 Apr 2025): Mitophagy-mediated S1P facilitates muscle adaptive responses to endurance exercise through SPHK1-S1PR1/S1PR2 in slow-twitch myofibers, Autophagy, DOI: 10.1080/15548627.2025.2488563

To link to this article: https://doi.org/10.1080/15548627.2025.2488563

AUTOPHAGY
https://doi.org/10.1080/15548627.2025.2488563

Taylor & Francis
Taylor & Francis Group

RESEARCH PAPER

OPEN ACCESS Check for updates

Mitophagy-mediated S1P facilitates muscle adaptive responses to endurance exercise through SPHK1-S1PR1/S1PR2 in slow-twitch myofibers

Minghong Leng[a], Fenghe Yang[a], Junhui Zhao[a], Yufei Xiong[a], Yiqing Zhou[a], Mingyang Zhao[a], Shi Jia[a], Limei Liu[a], Qiaoxia Zheng[a], Lebin Gan[b], Jingjing Ye[b], and Ming Zheng[a]

[a]Department of Physiology and Pathophysiology, School of Basic Medical Sciences, Peking University Health Science Center, and State Key Laboratory of Vascular Homeostasis and Remodeling, Peking University, Beijing, P.R. China; [b]Key Laboratory of Trauma Treatment and Neural Regeneration (Peking University), National Center for Trauma Medicine, Trauma Medicine Center, Peking University People's Hospital, Beijing, P.R. China

ABSTRACT

Endurance exercise triggers adaptive responses especially in slow-twitch myofibers of skeletal muscles, leading to the remodeling of myofiber structure and the mitochondrial network. However, molecular mechanisms underlying these adaptive responses, with a focus on the fiber type-specific perspective, remains largely unknown. In this study we analyzed the alterations of transcriptomics and metabolomics in distinct skeletal myofibers in response to endurance exercise. We determined that genes associated with sphingolipid metabolism, namely those encoding SPHK1, S1PR1, and S1PR2, are enriched in slow-twitch but not fast-twitch myofibers from both mouse and human skeletal muscles, and found that the SPHK1-S1PR pathway is essential for adaptive responses of slow-twitch to endurance exercise. Importantly, we demonstrate that endurance exercise causes the accumulation of ceramides on stressed mitochondria, and the mitophagic degradation of ceramides results in an increase of the sphingosine-1-phosphate (S1P) level. The elevated S1P thereby facilitates mitochondrial adaptation and enhances endurance capacity via the SPHK1-S1PR1/S1PR2 axis in slow-twitch muscles. Moreover, administration of S1P improves endurance performance in muscle atrophy mice by emulating these adaptive responses. Our findings reveal that the SPHK1-S1P-S1PR1/S1PR2 axis through mitophagic degradation of ceramides in slow-twitch myofibers is the central mediator to endurance exercise and highlight a potential therapeutic target for ameliorating muscle atrophy diseases.

ARTICLE HISTORY
Received 30 July 2024
Revised 7 January 2025
Accepted 31 March 2025

KEYWORDS
Endurance exercise; mitochondrial biogenesis; mitophagy; skeletal muscle; sphingosine-1-phosphate

Abbreviations CQ: chloroquine; DMD: Duchenne muscular dystrophy; EDL: extensor digitorum longus; FCCP: carbonyl cyanide p-trifluoromethoxyphenyl hydrazone; FUNDC1: FUN14 domain containing 1; GTEx: genotype-tissue expression; MYH: myosin heavy chain; mtDNA: mitochondrial DNA; PPARGC1A/PGC-1α: peroxisome proliferator activated receptor, gamma, coactivator 1 alpha; RG: red gastrocnemius; S1P: sphingosine-1-phosphate; S1PR: sphingosine-1-phosphate receptor; Sol: soleus; SPHK1: sphingosine kinase 1; TA: tibialis anterior; WG: white gastrocnemius

Introduction

Aerobic exercise capacity, as assessed through exercise stress testing, stands as one of the most robust predictors of physical well-being and overall mortality [1,2]. Epidemiological investigations have observed that reduced exercise capacity independently escalates the risk of cardiovascular diseases by up to 2–4 times [3,4], irrespective of other risk factors, such as age or obesity [5]. Two fundamental factors significantly influence exercise capacity and skeletal muscle function: the type of contractile fibers and energy metabolism [6]. Skeletal muscle myofibers are broadly categorized into slow-twitch (type I) and fast-twitch (type IIa, IIx, IIb) fibers based on the isoform of MYH (myosin heavy chain). Slow-twitch myofibers display exceptional resistance to fatigue and possess a substantial mitochondrial density, primarily relying on oxidative metabolism. In contrast, fast-twitch myofibers, although more powerful, tend to fatigue quickly and contain fewer mitochondria, predominantly depending on glycolytic metabolism [6]. Skeletal muscles exhibit remarkable adaptability, capable of structural and metabolic adjustments. Acute endurance exercise initiates mitochondrial energetic and oxidative stress, leading to subsequent adaptive responses, including autophagy and metabolic reprogramming [7,8]. Repeated and regular adaptive responses enhance fatigue resistance and increase the expression of proteins associated with mitochondrial metabolism in slow-twitch myofibers, ultimately enhancing overall muscle fitness [9,10]. Resistance exercise training, on the other hand, contributes to the

CONTACT Ming Zheng zhengm@bjmu.edu.cn Department of Physiology and Pathophysiology, School of Basic Medical Sciences, Peking University Health Science Center, and State Key Laboratory of Vascular Homeostasis and Remodeling, Peking University, Beijing 100191, P.R. China
Supplemental data for this article can be accessed online at https://doi.org/10.1080/15548627.2025.2488563

augmentation of both the proportion and cross-sectional area of fast-twitch myofibers, increasing muscle mass and strengthening strength [11]. Conversely, skeletal muscle dysfunction is mainly characterized by an aberrant shift in myofiber composition and defects in mitochondrial energy metabolism [12,13]. Previous studies indicate that muscle atrophy resulting from inactivity leads to a notable reduction in myofiber size, particularly affecting slow-twitch fibers. Additionally, a significant transition from type I and IIa (more slow-twitch) to type IIx (fast-twitch) fibers is observed under such conditions [14]. However, the aging process primarily affects fast-twitch myofibers, underscoring the importance of preserving fast-twitch myofiber mass and function to mitigate the effects of sarcopenia [15,16]. While variations in lipid metabolism and mitochondrial oxidative pathways have been identified as factors influencing fiber type-specific adaptive responses in slow and fast-twitch myofibers, the comprehensive molecular mechanisms governing these processes on a fiber type-specific basis remain elusive, necessitating further investigation and clarification.

Skeletal muscles have emerged as a secretory organ with a role in regulating metabolic homeostasis and body functions. Many cytokines (known as myokines) and metabolites (termed myometabolites) are released by muscles in response to exercise and exert their effects in autocrine, paracrine, or endocrine manners [17,18]. Exercise-induced myokines such as BDNF, FGF21, and FNDC5/Irisin promote mitochondrial biogenesis mediated by PPARGC1A/PGC-1α (peroxisome proliferator activated receptor, gamma, coactivator 1 alpha) and enhance bioenergetic balance in skeletal muscles [19]. FGF21 is released in response to mitochondrial stress during exercise, further emphasizing the role of signals originating from mitochondria in the adaptive responses [20]. In addition, exercise-induced metabolic changes lead to the release of bioactive metabolites within skeletal muscles. For instance, the prominent myometabolite lactate has been demonstrated to support muscle mass and enhance mitochondrial function [21,22]. Another metabolite, α-ketoglutaric acid, mediates the beneficial effects of exercise on muscle function and overall metabolic equilibrium [23].

Recently, a growing body of evidence suggests that macroautophagy/autophagy is activated during exercise and involved in the complex regulatory networks which coordinate adaptive responses to exercise [7,24]. A single bout of endurance exercise increases autophagy and mitophagy activity in mouse and human skeletal muscles [24–26]. Dysfunctional mitochondria are degraded through the autophagosome-lysosome pathway, which can boost mitochondrial OXPHOS function in skeletal muscle and enhance aerobic exercise capacity. Conversely, several muscle disorders including Duchenne muscular dystrophy (DMD) and age-related degeneration are characterized by impaired autophagy [27,28]. Furthermore, mice with a knockout of the mitochondrial autophagy receptor FUNDC1 (FUN14 domain containing 1) show impaired mitochondrial function in skeletal muscles and reduced endurance training adaptation [29]. Autophagy of subcellular structures releases a broad range of breakdown products – amino acids, fatty acids, and carbohydrates. These metabolites can be catabolized to maintain cellular energy equilibrium, or recycled to serve as substrates for macromolecule biosynthesis [7,30]. Nevertheless, little is known about the specific components of metabolites released from the breakdown of organelles like mitochondria and their potential roles as myometabolites.

Sphingolipids present in the membranous structure of cells and are bioactive phospholipids. Basically, sphingosine-1-phosphate (S1P) and ceramides are two bioactive sphingolipids which exert opposing effects on cellular processes. S1P is generated through the phosphorylation of sphingosine, a breakdown product of ceramides, by SPHK1 (sphingosine kinase 1) and SPHK2, and can be reversely transformed into ceramides [31,32]. S1P can act in paracrine or autocrine pathways, binding to a family of G-protein-coupled receptors known as S1P receptors (S1PR1 to S1PR5) to regulate downstream signaling. S1P usually promotes cell survival, proliferation, improves mitochondrial function, and enhances mitochondrial biogenesis [33], while ceramides are typically associated with pro-apoptotic signals and cellular stress responses [31]. The dynamic balance between these two molecules acts as a rheostat, finely tuning cellular responses and impacting various physiological outcomes. Alterations in this balance can significantly influence cell fate determination and have implications for health and disease states [32]. In skeletal muscles, S1P has been identified as a trophic factor to enhance muscle strength, mass, metabolism, and providing protection against fatigue [33–36]. However, S1P-S1PR3 signaling has also been reported to inhibit the regeneration in fast-twitch extensor digitorum longus (EDL) muscles after injury [37]. Additionally, although acute exhaustive exercise increases S1P levels in slow-twitch soleus (Sol) and red gastrocnemius (RG) muscles, it does not affect fast-twitch white gastrocnemius (WG) muscles [38], indicating that the impact of exercise on S1P levels varies depending on muscle types. Nevertheless, the mechanism underlying S1P production and its specific actions in different types of skeletal muscles remains unclear. In this study, we have identified S1P as a myometabolite originating from the mitophagic degradation of ceramides during endurance exercise, and the prevalence of the SPHK1-S1P-S1PR1/S1PR2 axis in slow-twitch myofibers contributes to the distinct adaptive responses of slow-twitch and fast-twitch muscles to endurance exercise.

Results

SPHK1-S1PRs are enriched in slow-twitch myofibers of mouse and human skeletal muscles

To identify possible transcriptomic disparities between slow-twitch and fast-twitch myofibers, we conducted Switching Mechanism at the 5' end of RNA Template-Seq (SMART-seq) analysis on single slow-twitch (type I) and fast-twitch (type IIb) myofibers isolated from mouse skeletal muscles. Slow-twitch myofibers were isolated from the Sol muscles, while fast-twitch myofibers were obtained from the EDL muscles. We at first compared transcriptomic changes of slow-twitch or fast-twitch myofibers from mice with or without endurance training (moderate-intensity treadmill running for 6 weeks). Heatmap showed substantial transcriptomic changes in slow-twitch myofibers after exercise comparing

with untrained ones, while fewer alterations were observed between trained and untrained fast-twitch myofibers (Figure 1A), suggesting that endurance training preferentially regulates slow-twitch but not fast-twitch myofibers. Further gene set enrichment analysis/GSEA revealed that exercise-caused changes in slow-twitch myofibers were pathways related to aerobic respiration, ribosome function, defense responses, and external encapsulating structures, while in fast-twitch myofibers were pathways associated with microtubule and supramolecular fiber organization (Figure S1A). Among these pathways, the classical adaptive responses to exercise including pathways associated with mitochondria, ribosome and fatty acid degradation were notably upregulated in slow-twitch myofibers (Figure S1B), indicating that endurance exercise result in a greater mitochondrial and metabolic remodeling in slow-twitch fibers than in fast-twitch fibers.

To uncover the potential molecular basis for the differential responsiveness of slow-twitch and fast-twitch myofibers to endurance exercise, we analyzed the transcriptomic profiles of the two types of myofibers. While the slow-twitch specific markers such as *Myh7*, *Myl3*, *Tnnt1* and *Tnni1* were enriched in slow-twitch myofibers, we noticed that genes associated with S1P metabolism and signals such as *Sphk1*, *S1pr1*, *S1pr2*, *S1pr3* and S1PR-coupled G proteins were also highly expressed in slow-twitch myofibers (Figure 1B). We then measured the expression of SPHK1 and S1PRs in slow-twitch Sol muscles and fast-twitch EDL muscles from mice. We found that both the protein and RNA levels of S1PR1, S1PR2, S1PR3 and SPHK1 were higher in slow-twitch muscles than in fast-twitch muscles (Figure 1C-D).

We further isolated slow- and fast-twitch myofibers from human hindlimb muscles. Consistently, mRNA levels of *S1PR1*, *S1PR2* and *SPHK1* in human slow-twitch (type I) myofibers were higher than in fast-twitch (type IIa) myofibers (Figure 1E). Co-immunostaining of SPHK1, S1PR1, or S1PR2 with MYH7 (type I) and MYH2 (type IIa) in human hindlimb muscle tissues revealed that SPHK1 was predominantly enriched in slow-twitch myofibers, and S1PR1 and S1PR2 were specifically located on the membranes of slow-twitch myofibers (Figure 1F). Together, these data identify the specific expression of SPHK1-S1PRs in slow-twitch but not fast-twitch myofibers in human and mouse skeletal muscles.

SPHK1-S1PR1/S1PR2 are required for the capacity of endurance exercise

By analyzing the transcriptomic profiles from the genotype-tissue expression (GTEx) dataset in human skeletal muscles, we found a significant positive correlation between SPHKs and S1PRs (Figure 2A). The transcriptomic profiles of mouse BXD strains [39] also revealed a significant positive correlation between the expression of *S1pr2* and *Sphk1* (Figure 2B). Principal component analysis (PCA) indicated that *S1pr2* and *Sphk1* were the primary contributors to the first principal component (PC1) (Figure S1C-D), and PC1 explained 38.1% of the variation in the expression of SPHKs-S1PRs pathway components (Figure 2C). Interestingly, PC1 score exhibited positive correlation with exercise training indicators. While the peak oxygen consumption rate (VO_2 max) during treadmill tests showed no significant correlation with the PC1 score in untrained BXD mice, it exhibited a positive correlation in BXD mice subjected to 6-week endurance training (Figure 2D). Likewise, the improvements in VO_2 max (ΔVO_2 max) and in running distance (Δrunning distance) also showed positive correlations after training (Figure 2D, Figure S1E). These data suggest that exercise-induced activation of the sphingolipid-related pathway may facilitate the adaptive responses in skeletal muscles.

Giving our finding that SPHK1-S1PRs is enriched in slow-twitch myofibers, we then investigated if the highly expressed SPHK1-S1PRs in slow-twitch myofibers accounts for the adaptive responses to endurance exercise. We used adeno-associated virus (AAV) serotype 9 for intramuscular (i.m.) delivery of short hairpin RNA (shRNA) of *Sphk1*, *S1pr1* or *S1pr2* under the control of a ubiquitous promoter U6. 6-week treadmill training was performed 2 weeks after the AAV9 injection (Figure 2E). AAV9-shRNAs led to a significant reduction in mRNA and protein levels of SPHK1, S1PR1 or S1PR2 in gastrocnemius (Gas) and Sol muscles (Figure S2A-B). Mice injected with AAV9-sh*Sphk1*, sh*S1pr1* or sh*S1pr2* exhibited the decreased running population of mice, shorter running time, decreased running distance and decreased work accomplished until exhaustion during treadmill stress (Figure 2F-I). We further administered the mice with S1PR inhibitors W146, JTE-013, or CAY10444 (Figure S2C), and treadmill stress tests showed that inhibition of S1PR1 by W146 or inhibition of S1PR2 by JTE-013 caused decreased endurance capacity, decreased running population of mice, shorter running time, decreased running distance, and decreased work to exhaustion, while inhibition of S1PR3 by CAY10444 showed no significant alterations, as compared with control mice (Figure 2J-M). Taken together, these findings suggest that SPHK1-S1PR1/S1PR2 axis plays a pivotal role in the adaptation to endurance exercise.

SPHK1-S1PR1/S1PR2 mediate mitochondrial adaptation to endurance exercise in slow-twitch muscles

Our SMART-seq data showed that exercise-caused notable upregulation of the classical adaptive responses to exercise including pathways associated with aerobic respiration and mitochondria in slow-twitch myofibers (Figure S1A-B), so we measured the protein levels of mitochondrial OXPHOS complexes and mitochondrial DNA (mtDNA) copies in slow-twitch and fast-twitch muscles from *Sphk1*, *S1pr1* or *S1pr2* silencing mice after endurance exercise. Muscle-specific knockdown of *Sphk1*, *S1pr1* or *S1pr2* significantly reduced protein levels of complexes I-V and mtDNA copies in slow-twitch Sol and RG muscles (Figure 3A-D), but not in fast-twitch WG muscles (Figure 3E-F). PPARGC1A/PGC-1α, the master regulator of mitochondrial biogenesis was also decreased in *Sphk1* and *S1pr2* knockdown slow-twitch muscles, but not in fast-twitch muscles (Figure 3A, C, E). Although *S1pr1* knockdown did not change PPARGC1A level in both slow-twitch and fast-twitch muscles. Likewise, inhibition of S1PR1 by W146 and S1PR2 by JTE-013 caused decreased mitochondrial OXPHOS

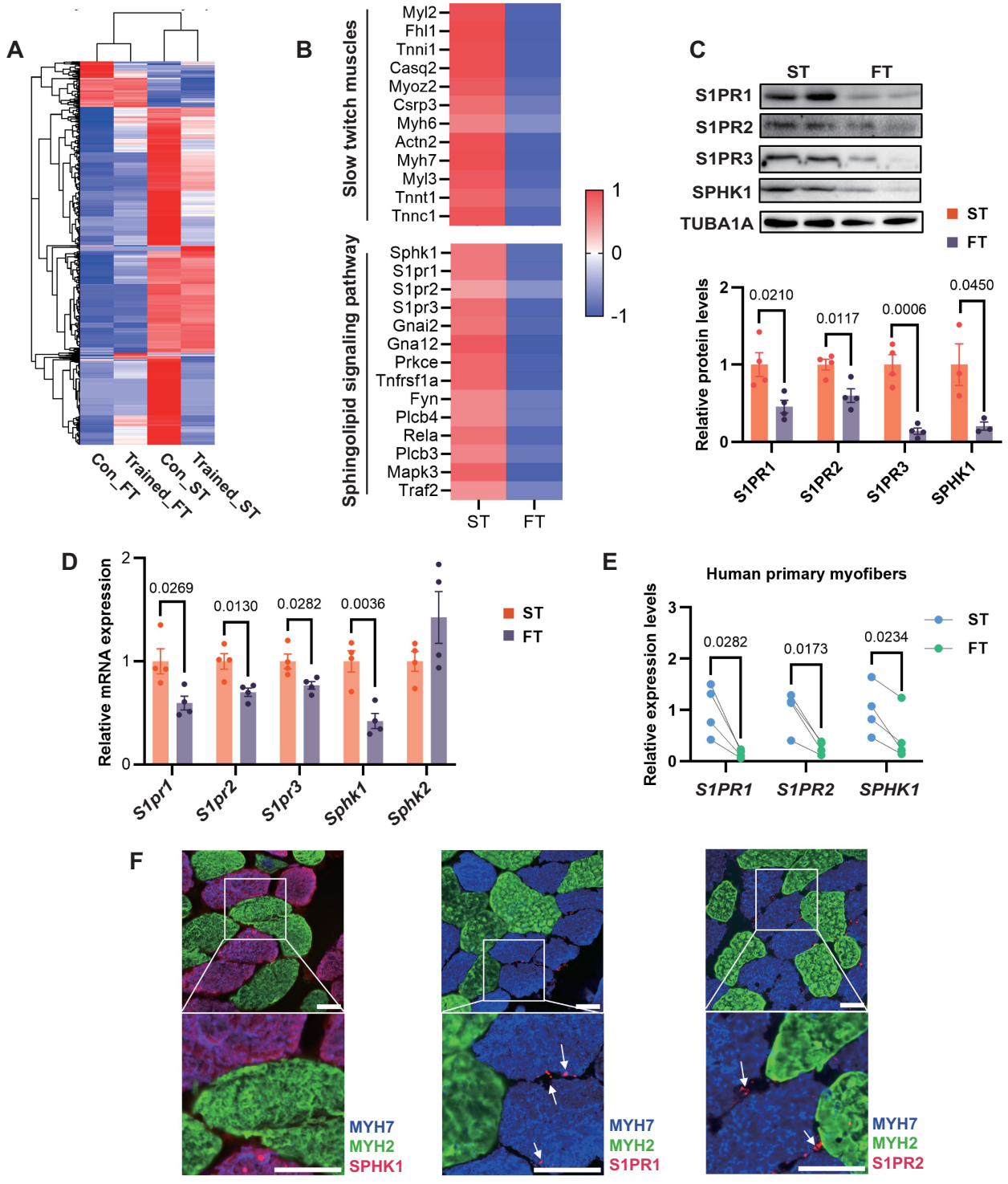

Figure 1. SPHK1 and S1PRs are enriched in slow-twitch myofibers. (A) Heatmap showing relative expression (red, high; blue, low) detected by smart-seq of mRNA from slow-twitch (ST) and fast-twitch (FT) myofibers isolated from trained and untrained mice ($n = 3$). Con_FT, type IIb fiber isolated from control EDL. Trained_FT, type IIb fiber isolated from endurance exercise trained EDL. Con_ST, type I fiber isolated from control soleus. Trained_ST, type I fiber from endurance exercise trained soleus. (B) Heatmap showing relative expression levels of slow-twitch muscle-related genes and sphingolipid signaling-related genes in slow- and fast-twitch myofibers. (C) Protein levels of S1PR1, S1PR2, S1PR3 and SPHK1 in mouse slow- (sol) and fast-twitch (EDL) muscles ($n = 3$–4). (D) qPCR analysis of *S1pr1*, *S1pr2*, *S1pr3*, *Sphk1* and *Sphk2* mRNA levels in mouse slow- (sol) and fast-twitch (EDL) muscles ($n = 4$). (E) qPCR analysis of *S1PR1*, *S1PR2* and *SPHK1* mRNA levels in isolated slow- and fast-twitch myofibers from human hindlimb muscle tissues ($n = 4$). (F) Co-immunostaining of SPHK1, S1PR1, or S1PR2 with MYH7 (type I) and MYH2 (type IIa) in human hindlimb muscle tissues. Scale bar: 50 μm. All data are shown as the means ± SEM. Differences between two groups were assessed using two-tailed student's t tests.

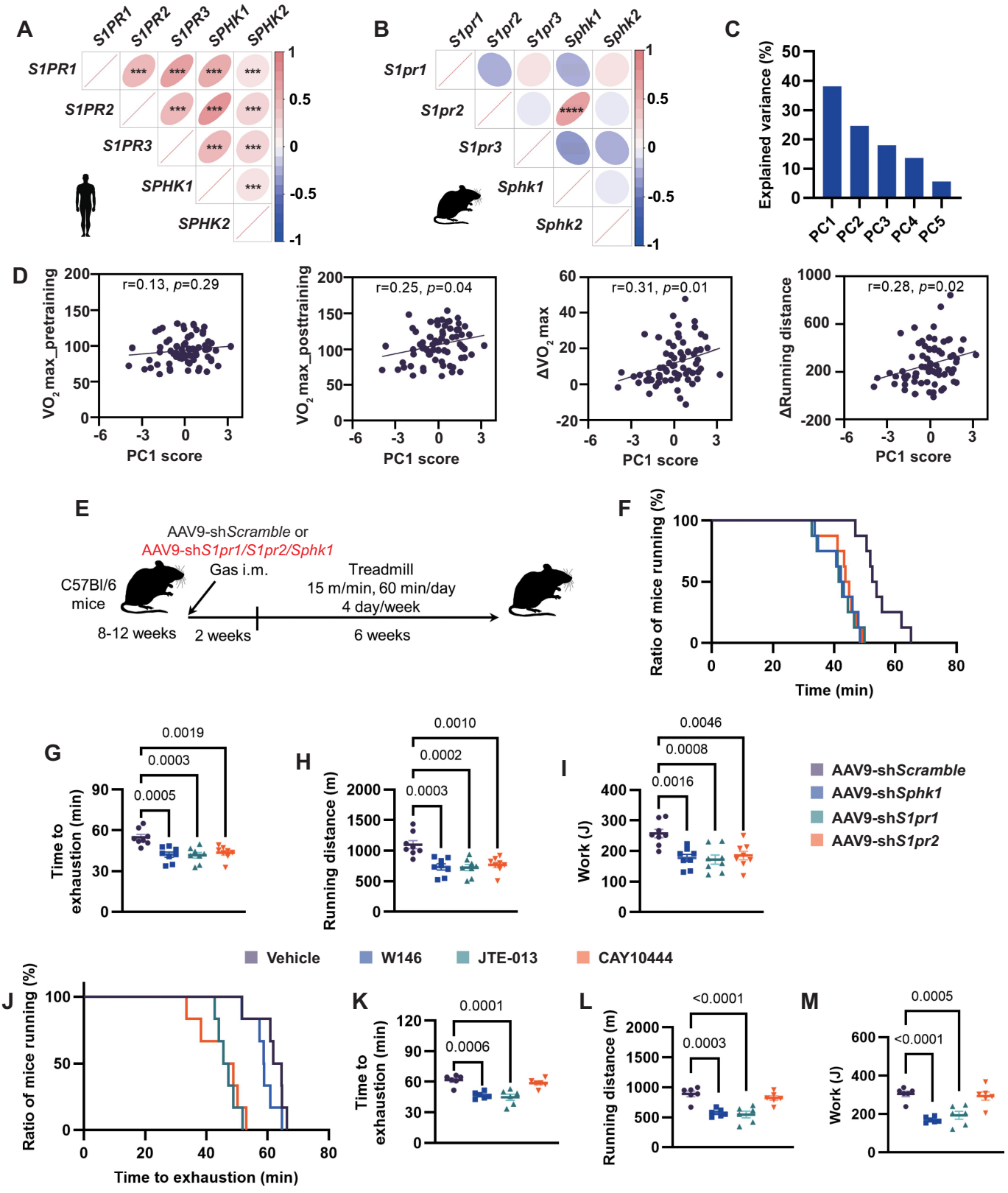

Figure 2. SPHK1-S1PR1/S1PR2 are required for the capacity of endurance exercise. (A) Correlation heatmap plot of expression of SPHKs and S1PRs in human skeletal muscles (GTEx, $n = 803$). The colors of ellipses represent Pearson's coefficient. ***$p < 0.001$. (B) Correlation heatmap plot of expression of SPHKs and S1PRs in skeletal muscles of 35 genetically diverse BXD strains. The colors of ellipses represent Pearson's coefficient. ****$p < 0.0001$. (C) Proportion of variance explained by principal components of the S1P signaling pathway. (D) Pearson's correlation of PC1 score with endurance performance traits in 35 genetically diverse BXD strains. (E-I) 8-week-old male C57BL/6J mice were intramuscularly injected with AAV9-shScramble, AAV9-sh*Sphk1*, AAV9-sh*S1pr1* or AAV9-sh*S1pr2* in bilateral gastrocnemius. 2 weeks after intramuscular injection, mice were subjected to treadmill training for 6 weeks. (E) Experimental scheme. (F) running population of trained mice during treadmill stress test ($n = 8$). (G-I) Running time (G), distance (H) and work (I) performed until exhaustion during treadmill stress test ($n = 8$). (J-M) 8-week-old male C57BL/6J mice were subjected to 6-week treadmill training and treated with intraperitoneal injections of vehicle (4 mg/mL BSA in normal saline), W146 (5 mg/kg, every other day), JTE-013 (5 mg/kg, every other day) or CAY10444 (5 mg/kg, every other day) for 6 weeks. Running population (J), running time (K), distance (L) and work (M) performed until exhaustion during treadmill stress test ($n = 6$). All data are shown as the means ± SEM. Differences for more than two groups were assessed using one-way ANOVA with Tukey's post hoc test.

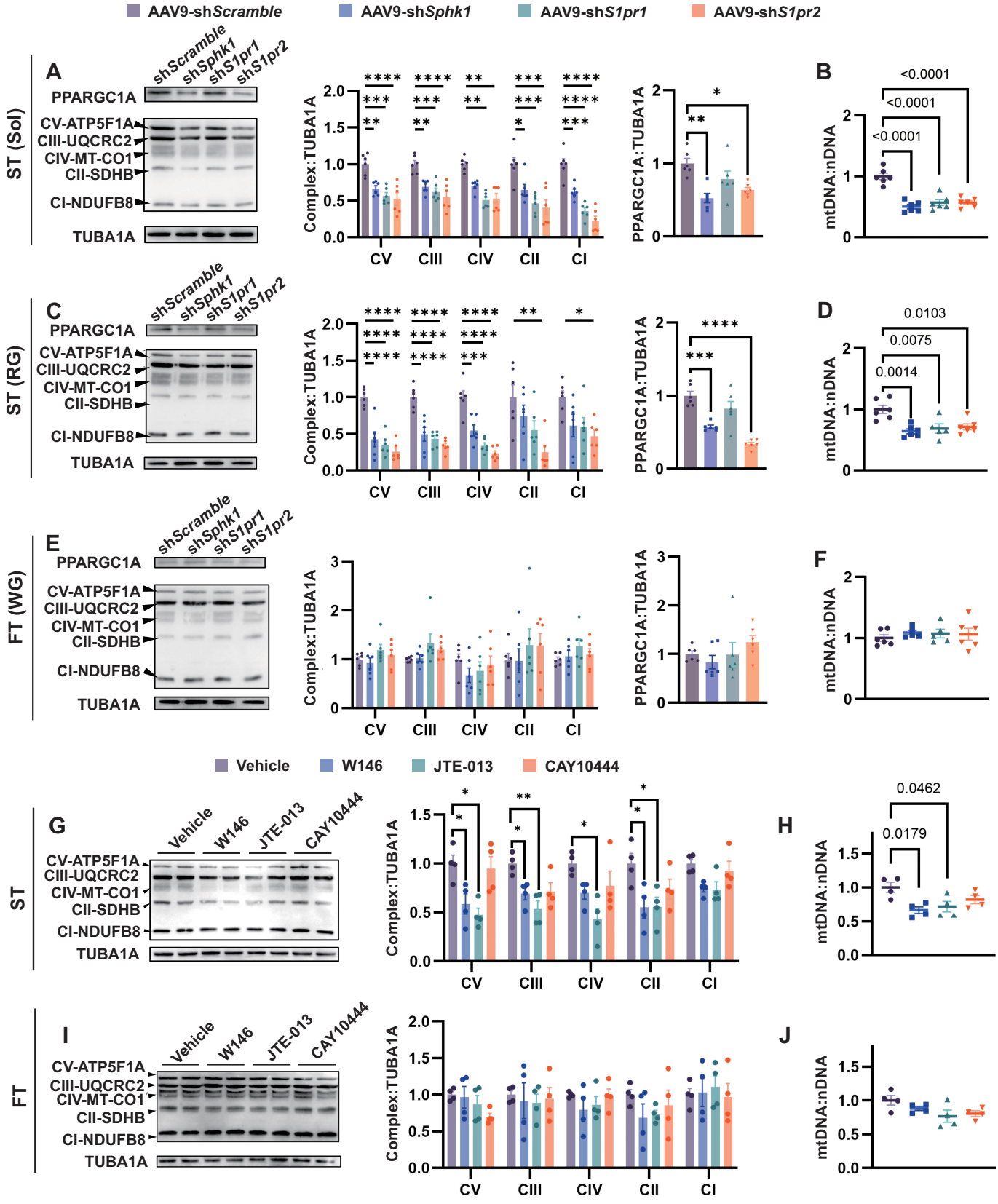

Figure 3. SPHK1-S1PR1/S1PR2 mediate mitochondrial adaptation to endurance exercise in slow-twitch muscles. (A-F) 8-week-old male C57BL/6J mice were intramuscularly injected with AAV9-shScramble, AAV9-sh*Sphk1*, AAV9-sh*S1pr1* or AAV9-sh*S1pr2* in bilateral gastrocnemius muscles. 2 weeks after intramuscular injection, mice were subjected to treadmill training for 6 weeks. (A) Protein levels of OXPHOS complexes and PPARGC1A in slow-twitch muscles (sol) (n = 6). (B) Ratios of mtDNA:nDNA measured by qPCR in slow-twitch muscles (sol) (n = 6). (C) Protein levels of OXPHOS complexes and PPARGC1A in slow-twitch muscles (RG) (n = 6). (D) Ratios of mtDNA:nDNA measured by qPCR in slow-twitch muscles (RG) (n = 6). (E) Protein levels of OXPHOS complexes and PPARGC1A in fast-twitch muscles (WG) (n = 6). (F) Ratios of mtDNA:nDNA measured by qPCR in fast-twitch muscles (WG) (n = 6). (G-J) 8-week-old male C57BL/6J mice were subjected to 6-week treadmill training and treated with intraperitoneal injections of vehicle (4 mg/mL BSA in normal saline), W146 (5 mg/kg, every other day), JTE-013 (5 mg/kg, every other day) or CAY10444 (5 mg/kg, every other day) for 6 weeks. (G) Protein levels of OXPHOS complexes in slow-twitch muscles (sol) (n = 4). (H) Ratios of mtDNA:nDNA measured by qPCR in slow-twitch muscles (sol) (n = 4). (I) Protein levels of OXPHOS complexes in fast-twitch muscles (EDL) (n = 4). (J) Ratios of mtDNA:nDNA measured by qPCR in fast-twitch muscles (EDL) (n = 4). All data are shown as the means ± SEM. Differences for more than two groups were assessed using one-way ANOVA with Tukey's post hoc test. *p* value are indicated as follows: *$p < 0.05$, **$p < 0.01$. ***$p < 0.001$, ****$p < 0.0001$.

complexes I-V and mtDNA copies in slow-twitch Sol muscles but not in fast-twitch EDL muscles (Figure 3G-J). Taken together, these data suggest that SPHK1-S1PRs mediated endurance exercise capacity may be through regulating the mitochondrial adaptation specifically in slow-twitch muscles.

S1P is increased in slow-twitch myofibers and regulates mitochondrial adaptation to endurance exercise in mouse and human skeletal muscles

Next, we analyzed possible metabolomics changes in slow-twitch muscles isolated from sedentary and exercised mice by LC-MS/MS, and the data showed prominently ranked sphingolipid mediator S1P (Figure 4A). We further found that S1P abundance was increased in slow-twitch Sol and RG muscles during acute moderate-intensity exercise and even 3 h after exercise, but showed no difference in fast-twitch EDL and tibialis anterior (TA) muscles before and after exercise (Figure 4B and Figure S3A). Because bioactive S1P links SPHK1 with S1PRs in sphingolipid signaling pathway, the finding that S1P is specifically increased in slow-twitch myofibers after exercise is in consistent with the high expression level of SPHK1-S1PRs in slow-twitch myofibers, suggesting that endurance exercise may increase S1P and improve the exercise capacity through SPHK1-S1PRs in slow-twitch myofibers.

We then injected S1P intraperitoneally into male C57BL/6J mice to test the function of S1P on muscle adaptation to endurance exercise in vivo (Figure S3B). S1P injection increased mouse exercise capacity as indicated by the increased number of running individuals, longer running time, and increased work accomplished until exhaustion during treadmill stress (Figure 4C-E). Importantly, we found that S1P treatment only enhanced PPARGC1A protein levels and mtDNA copies in slow-twitch Sol and RG muscles but not in fast-twitch EDL and TA muscles (Figure 4F-M). Moreover, immunostaining of the soleus muscle revealed that S1P administration even promoted an increase in the proportion of type I myofibers (Figure 4N), indicating that the fibers could be switched to the mitochondria-rich slow-twitch type in response to S1P. These results suggest that S1P increase exercise capacity through improving mitochondrial adaptation specifically in slow-twitch myofibers.

We also measured the effect of S1P on mitochondrial function in human primary myotubes. S1P treatment largely increased basal mitochondrial respiration and maximal respiratory capacity (Figure 4O-P), and caused increased protein levels of OXPHOS complexes and PPARGC1A, along with increased mtDNA copies (Figure 4Q-R). Likewise, S1P improved mitochondrial biogenesis and respiratory capacity in C2C12 mouse myotubes (Figure S3C-G). Taken together, these *in vivo* and *in vitro* data further suggest that the specifically increased S1P in slow-twitch myofibers contributes to the mitochondrial adaptation in response to endurance exercise.

Mitophagic degradation of ceramides during exercise generates S1P and facilitates mitochondrial biogenesis through SPHKs-S1P-S1PRs in skeletal muscles

S1P is produced through the phosphorylation of sphingosine by SPHK1/SPHK2, while sphingosine is derived from the hydrolysis of ceramides by ceramidases (Figure 5A). To understand the origin of the increased S1P in slow-twitch myofibers in response to endurance exercise, we examined levels of sphingosine and ceramide by quantitative LC-MS/MS analysis in slow-twitch RG muscles from mice after treadmill running. We found that both sphingosine and S1P levels were increased during exercise and 3 h after exercise comparing with untrained control muscles. Although the abundance of ceramides is much more than that of S1P, ceramides in whole-tissue extract did not significantly change (Figure 5B). Interestingly, further measuring ceramide levels in the mitochondria-enriched fraction of slow-twitch RG muscles, we found a significant increase in C18-ceramides during exercise and returning to baseline at 3 h after exercise (Figure 5B), suggesting that the small proportion of mitochondrial ceramide change may contribute to the change of sphingosine and S1P.

In cancer cells it has been reported that ceramides accumulated on mitochondria under stress conditions to mediate mitophagy [40–42]. We then detected the possible mitochondrial accumulation of ceramides in C2C12 myotubes stimulated with the protonophore carbonyl cyanide p-trifluoromethoxyphenyl hydrazone (FCCP) to induce mitochondrial stress. While FCCP caused the redistribution of autophagy maker MAP1LC3/LC3 into puncta around mitochondria, it increased the colocalization of ceramides with both mitochondria and LC3 (Figure 5C), supporting that ceramides accumulate on stressed mitochondria in myotubes. Thus, we hypothesized that exercise induces mitochondrial stress which causes the accumulation of ceramides on mitochondria and the subsequent mitophagy result in the hydrolysis of ceramides by acid ceramidase in lysosomes. We at first utilized mice expressing mt-Keima, a pH-dependent fluorescent indicator of mitophagy, to detect the mitophagy in skeletal muscles in response to endurance exercise [43,44]. Indeed, mitophagy was significantly increased, as indicated by the shifted excitation spectrum of mt-Keima from 488 nm to 552 nm (Figure S4A-C), and also by the increased protein levels of LC3-II in both whole cell lysates and mitochondria-enriched fraction from exercised slow-twitch RG muscles (Figure S4D-E), suggesting that endurance exercise causes elevated mitophagy in slow-twitch muscles. Then, we employed mitophagy receptor *fundc1* knockout (KO) mice to investigate the effect of mitophagy deficiency on ceramides and S1P in response to endurance exercise. The *fundc1* KO resulted in decreased protein levels of mitochondrial LC3-II in slow-twitch RG muscles with/without exercise training comparing with control mice (Figure S4F). Unlike in wild-type muscles, sphingosine and S1P levels were not increased in response to exercise in slow-twitch RG muscles of *fundc1* KO mice (Figure 5D), suggesting that mitophagy deficiency blocks the exercise-induced increase of sphingosine and S1P

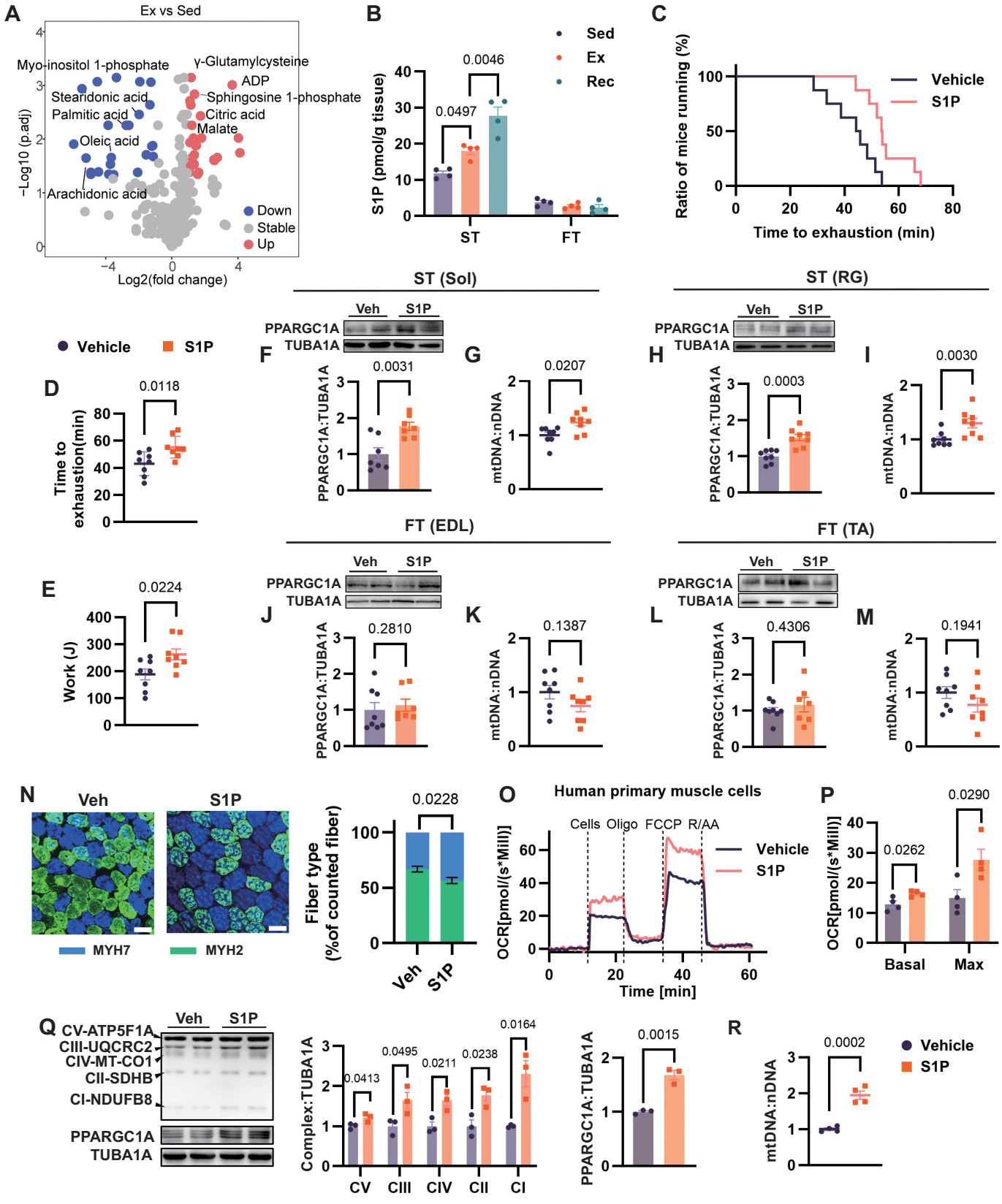

Figure 4. Increased S1P in slow-twitch myofibers mediates mitochondrial adaptation to endurance exercise in mouse and human skeletal muscles. (A) Volcano plot showing the metabolite abundance in sedentary (sed) and acute exercised (ex) slow-twitch muscles. Differentially regulated metabolites are marked in blue (downregulated in exercised muscles) and red (upregulated in exercised muscles). (B) Quantification of S1P concentrations in slow- (sol) and fast-twitch (EDL) muscles from mice at rest (sed), during acute exercise (ex) and recovering for 3 h after exercise (rec) ($n = 4$). (C-N) 8-week-old male C57BL/6J mice were treated with intraperitoneal injections of S1P for 4 weeks (1 mg/kg, every other day). (C-E) Running population (C), running time (D) and work (E) performed until exhaustion of mice during treadmill stress test ($n = 8$). (F) protein levels of PPARGC1A in slow-twitch muscles (sol) ($n = 7$). (G) Ratios of mtDNA:nDNA measured by qPCR in slow-twitch muscles (sol) ($n = 8$). (H) Protein levels of PPARGC1A in slow-twitch muscles (RG) ($n = 8$). (I) ratios of mtDNA:nDNA measured by qPCR in slow-twitch muscles (RG) ($n = 8$). (J) protein levels of PPARGC1A in fast-twitch muscles (EDL) ($n = 7$–8). (K) Ratios of mtDNA:nDNA measured by qPCR in fast-twitch muscles (EDL) ($n = 7$–8). (L) Protein levels of PPARGC1A in fast-twitch muscles (TA) ($n = 7$–8). (M) Ratios of mtDNA:nDNA measured by qPCR in fast-twitch muscles (TA) ($n = 7$–8). (N)

in slow-twitch muscles. The *fundc1* KO mice also exhibited reduced endurance capacity and diminished adaptability to endurance exercise, as indicated by decreased running time and work during treadmill test as well as limited improvement after 6-week endurance training (Figure S4G-J). In contrast to the unchanged sphingosine and S1P level, C18-ceramides were still increased in mitochondria-enriched fraction from *fundc1* KO slow-twitch muscles during exercise, but lasting at even higher level and not returning to basal level until 3 h after exercise (Figure 5D), suggesting that the mitophagy deficiency inhibits the degradation of accumulated C18-ceramides on stressed mitochondria. Actually, in C2C12 myotubes, we detected that blockage of the autophagy degradation by the autophagy inhibitor chloroquine (CQ) slightly increased the co-localization of ceramides with mitochondria and LC3, and largely increased the co-localization after FCCP stimulation (Figure S5A), further supporting that ceramides accumulate on stressed mitochondria and inhibition of mitophagy degradation aggravates the detained ceramides on stressed mitochondria. Consistently, in C2C12 myotubes FCCP increased sphingosine and S1P levels and the increase was abolished by CQ pretreatment (Figure 5E). FCCP caused accumulation of C16/18-ceramides in the mitochondria-enriched fraction and pretreatment with CQ further elevated FCCP-increased ceramides (Figure 5E). Furthermore, inhibition of acid ceramidase by NOE or inhibition of SPHKs by SKI-II significantly blocked FCCP-induced increase of S1P (Figure 5F). Together, these data suggest that ceramides accumulate on stressed mitochondria during endurance exercise and the mitophagic degradation of ceramides causes increased sphingosine and S1P in slow-twitch muscles.

Next, we investigated the effect of mitophagy-mediated S1P on mitochondrial function in C2C12 myotubes. FCCP treatment caused decreased mtDNA copies which was recovered 48 h after FCCP elution (Figure S5B), indicating the recovery of mitochondria 48 h after mitophagy. We found that PPARGC1A protein level was increased 48 h after FCCP stimulation, pretreatment with CQ, NOE, or SKI-II blocked the upregulation of PPARGC1A and S1P restored FCCP-mediated PPARGC1A (Figure 5G-I). Consistently, CQ, NOE, or SKI-II significantly reduced mitochondrial turnover ratio, as indicated by mtDNA recovery at 48 h after FCCP stimulation, and S1P restored it (Figure S5C). Furthermore, silencing *Sphk1* and *Sphk2* by siRNAs blocked both exogenous sphingosine and FCCP-induced increase of PPARGC1A and mtDNA recovery, while S1P restored FCCP-induced PPARGC1A and mtDNA recovery (Figure S5D-F). Together, these data suggest that S1P from mitophagic degradation of ceramide contributes to mitochondrial biogenesis.

Since S1P can act in paracrine or autocrine pathways, we then tested effects S1PRs on mitophagy-mediated S1P function. We found that inhibition of S1PR2 by siRNA or by inhibitor JTE-013 notably inhibited the FCCP-induced increase of PPARGC1A and mitochondrial turnover ratio (Figure 5J-M), inhibition of S1PR1 and S1PR3 did not change FCCP-induced increase of PPARGC1A although S1PR1 inhibition reduced FCCP-induced mitochondrial turnover (Figure 5J-M and Figure S5G-H). Collectively, our findings suggest that the mitophagic degradation of ceramides during exercise causes increased S1P in slow-twitch muscles and facilitates mitochondrial biogenesis through SPHKs-S1P-S1PRs.

S1P improves the mitochondrial adaptation in slow-twitch muscles and the endurance capacity of disuse atrophy mice

To determine the pathophysiological relevance of SPHK-S1P-S1PRs pathway in skeletal muscles, we analyzed publicly available transcriptome data from a collection of human muscle aging, myopathy, and dystrophy datasets. Intriguingly, we found notable decreases in the expression levels of *S1PR1/S1PR2* and *SPHK1* in patients with skeletal muscle diseases and in aging individuals (Figure 6A), suggesting the potential involvement of declined S1P signaling in disease-related skeletal muscle dysfunction.

We then established a muscle disuse atrophy mouse model with 2 weeks of hindlimb immobilization, and the mice were intraperitoneally injected with S1P or vehicle as control (Figure 6B). Compared with control mice, immobilized mice exhibited decreased endurance performance as indicated by decreased running population, shorter running time, and work until exhaustion, S1P administration largely improved endurance performance (Figure 6C-E). Interestingly, 2-week immobilization caused loss of muscle mass in the slow-twitch soleus and mixed gastrocnemius muscles but not in fast-twitch EDL and TA muscles, while S1P largely rescued the muscle loss (Figure 6F). Furthermore, administration of S1P resulted in the upregulation of PPARGC1A, OXPHOS complexes, and mtDNA copies specifically in slow-twitch but not fast-twitch muscles of immobilized mice (Figure 6G-L and Figure S6A-F), in accordance with our finding that the S1P related SPHK1-S1PRs axis is highly expressed in slow-twitch myofibers. Notably, we observed that S1P also induced a transformation of myofiber types within the slow-twitch Sol and RG muscles, shifting from fast- to slow-twitch type, particularly in immobilized mice (Figure 6M and Figure S6C). In contrast, no fiber type transformation was observed in the fast-twitch EDL and TA muscles in response to S1P (Figure 6N and Figure S6F). Together, these findings suggest that S1P administration improves endurance performance in

Representative images and quantification of fiber type staining of slow-twitch muscles (sol) ($n = 6$). Blue, MYH7 (type I); green, MYH2 (type IIa). Scale bar: 50 μm. (O-R) Human primary myoblasts were differentiated for 5 days and then treated with vehicle (4 mg/mL BSA in DMEM) or S1P (5 mm) for 48 h. (O-P) Representative traces and quantification of mitochondrial respirometry of the human primary muscle cells ($n = 4$). (Q) Protein levels of OXPHOS complexes and PPARGC1A in the human primary muscle cells ($n = 3$). (R) Ratios of mtDNA:nDNA measured by qPCR in the human primary muscle cells ($n = 4$). All data are shown as the means ± SEM. Differences between two groups were assessed using two-tailed student's t tests (D-R). Differences for more than two groups were assessed using one-way ANOVA with Tukey's post hoc test (B).

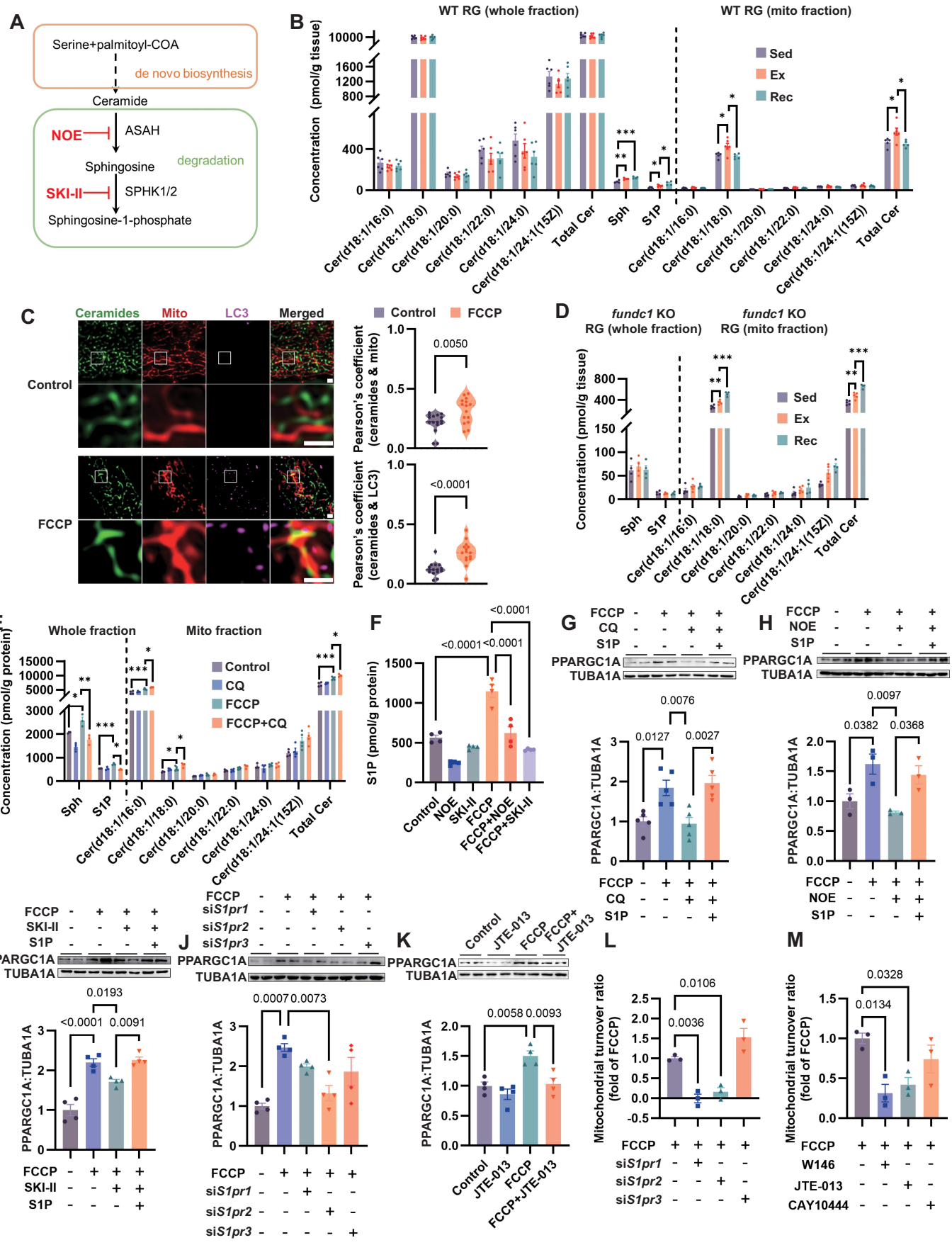

Figure 5. Mitophagic degradation of ceramides during exercise generates S1P and facilitates mitochondrial biogenesis through SPHKs-S1P-S1PRs in skeletal muscles. (A) Schematic representation of the ceramide-S1P metabolism. (B) Quantification of sphingosine, S1P and ceramide concentrations in whole fraction and mitochondrial fraction of slow-twitch muscles (RG) from WT mice at rest (sed), during exercise (ex) and recovering for 3 h after exercise (rec) (n = 4–6). (C) Representative immunofluorescence images and Pearson's correlation coefficients of ceramide (green), MitoTracker (red) and LC3 (magenta) in C2C12 cells treated

disuse atrophy mice possibly through increasing mitochondrial adaptation in slow-twitch muscles.

Discussion

In this study, we identified that SPHK1-S1P-S1PRs axis primarily functions in slow-twitch muscles, regulating adaptive responses to endurance exercise. We found that SPHK1-S1PR1/S1PR2 were highly expressed in slow-twitch but not fast-twitch myofibers in mouse and human skeletal muscles, and were required for adaptive responses of slow-twitch muscles to endurance exercise. Mechanically, endurance exercise caused the accumulation of ceramides on stressed mitochondria, and the mitophagic degradation of ceramides increased S1P, which in turn facilitated mitochondrial biogenesis and muscle performance in slow-twitch muscles of human and mice. SPHK1-S1PR1/S1PR2 expression is decreased in the skeletal muscles of patients with muscle disorders, injection of S1P caused significant activation of mitochondrial biogenesis specifically in slow-twitch muscles and improved endurance performance of disuse atrophy mice. Collectively, our *in vivo* and *in vitro* data demonstrate that the mitophagy-mediated degradation of ceramides increases S1P which plays a critical role in mitochondrial adaptation and endurance performance in response to endurance exercise through SPHK1-S1PR1/S1PR2 in slow-twitch muscles.

Previous studies with whole-muscle samples revealed a combination of various myofiber types [45,46]. Taking advantage of single-cell techniques, which facilitate the identification of transcriptional patterns that govern the functional and metabolic traits of individual myofiber types [47], our present study revealed different transcriptomic profiles in slow-twitch and fast-twitch myofibers under sedentary conditions and in response to endurance training. Compared to fast-twitch myofibers, endurance training resulted in enhanced signals associated with typical exercise adaptive responses, including fatty acid oxidation, mitochondrial biogenesis, and protein synthesis in slow-twitch myofibers. SMART-seq analysis of single myofibers in mice demonstrated that these differences in response to endurance training might be attributed to the higher expression levels of genes involved in the S1P signaling related pathway in slow-twitch than fast-twitch myofibers. Notably, SPHK1 and S1PR1/S1PR2 were highly expressed in slow-twitch myofibers in both human hindlimb muscles and mouse skeletal muscles. The higher expression levels of SPHK1 contribute to the local increase in S1P specifically in slow-twitch muscles during exercise. S1P acts in an autocrine or paracrine manner via S1PR1/S1PR2 on the plasma membrane of slow-twitch muscles to mediate mitochondrial adaptation. These findings are supported by a previous study showing an increase in S1P levels in exercised rat Sol and RG muscles but not in WG muscles [38]. Through genetic analysis of human GTEx database and mouse BXD strains we noticed the strong positive correlation between the expression levels of SPHK1 and S1PR2, which was positively associated with endurance performance and training-induced improvements. By genetically silencing or pharmacologically inhibiting SPHK1, S1PR1, or S1PR2, we found that endurance training-induced mitochondrial biogenesis were blocked especially in slow-twitch muscles, confirming the notion that the highly expressed SPHK1-S1PR1/S1PR2 in slow-twitch myofibers plays a central role in mediating mitochondrial adaptation to endurance exercise.

Our present study identified mitophagy as a crucial pathway responsible for regulation of the ceramide-S1P rheostat in skeletal muscles. Endurance exercise results in accumulation of ceramides on mitochondria, and the elevated mitochondrial ceramides are involved in mitophagy. We observed increased mitochondrial ceramide abundance and increased mitophagy in exercised mouse RG muscles. Consistently, FCCP-treated C2C12 myotubes exhibited colocalization of LC3 and mitochondrial ceramides, supporting the role of ceramides as a mitophagy receptor. Mitophagy deficiency induced by knockout of FUNDC1 [29] or inhibition of mitophagy degradation with CQ aggravated the accumulation of ceramides on mitochondria in muscle cells during exercise or FCCP stimulation. This excessive accumulation of ceramides on mitochondria may contribute to reduced endurance training adaptation and potential muscle damage caused by excessive exercise [48]. The mitophagic hydrolysis of ceramides leads to the production of S1P in slow-twitch muscles during endurance exercise. *fundc1* KO, CQ treatment, and acid ceramidase inhibition all abolished the increase of S1P in response to endurance exercise or to FCCP stimulation, providing evidence to support our notice that the increased S1P during endurance exercise is produced from the hydrolyzed ceramides by mitophagic degradation in lysosome. Our finding is supported by previous studies in patients with Niemann-Pick type C, a lysosome storage disease characterized by sphingolipid metabolism disorders, the production of S1P and S1PR1-KLF2-ETV1-

with or without 10 μM FCCP (n = 12–16 cells from 3 biological replicates for every group). Scale bar: 2 μm. (D) Quantification of sphingosine, S1P and ceramide concentrations in whole fraction and mitochondrial fraction of slow-twitch muscles (RG) from *fundc1* KO mice at rest (sed), during exercise (ex) and recovering for 3 h after exercise (rec) (n = 4–5). (E) quantification of sphingosine, S1P and ceramide concentrations in whole fraction and mitochondrial fraction of C2C12 myotubes treated with 10 μM FCCP, in the absence or presence of 50 μM CQ pre-treatment (n = 4–5). (F) Quantification of S1P concentrations in C2C12 myotubes treated with 10 μM FCCP for 4 h with/without 50 μM NOE or 5 μM SKI-II pre-treatment (n = 4). (G) PPARGC1A protein levels in the C2C12 myotubes 48 h after the stimulation of 10 μM FCCP with/without 50 μM CQ in the absence or presence of 5 μM S1P (n = 5). (H) PPARGC1A protein levels in the C2C12 myotubes 48 h after the stimulation of 10 μM FCCP with/without 50 μM NOE in the absence or presence of 5 μM S1P (n = 3). (I) PPARGC1A protein levels in the C2C12 myotubes 48 h after the stimulation of 10 μM FCCP with/without 5 μM SKI-II in the absence or presence of 5 μM S1P (n = 4). (J) PPARGC1A protein levels in si*NC*, si*S1pr1*, si*S1pr2* or si*S1pr3* transfected C2C12 myotubes 48 h after the stimulation of 10 μM FCCP (n = 4). (K) PPARGC1A protein levels in C2C12 myotubes treated with 10 μM JTE-013 for 48 h after the stimulation of 10 μM FCCP (n = 4). (L) Mitochondrial turnover ratio of si*NC*, si*S1pr1*, si*S1pr2* or si*S1pr3* transfected C2C12 myotubes 48 h after the stimulation of 10 μM FCCP (n = 3). (M) Mitochondrial turnover ratio of C2C12 myotubes treated with 10 μM JTE-013, 5 μM W146 or 10 μM CAY10444 for 48 h after the stimulation of 10 μM FCCP (n = 3). All data are shown as the means ± SEM. Differences between two groups were assessed using two-tailed student's t tests (C). Differences for more than two groups were assessed using one-way ANOVA with Tukey's post hoc test (B, D-M). *p* values are indicated as follows: **p* < 0.05, ***p* < 0.01. ****p* < 0.001, *****p* < 0.0001.

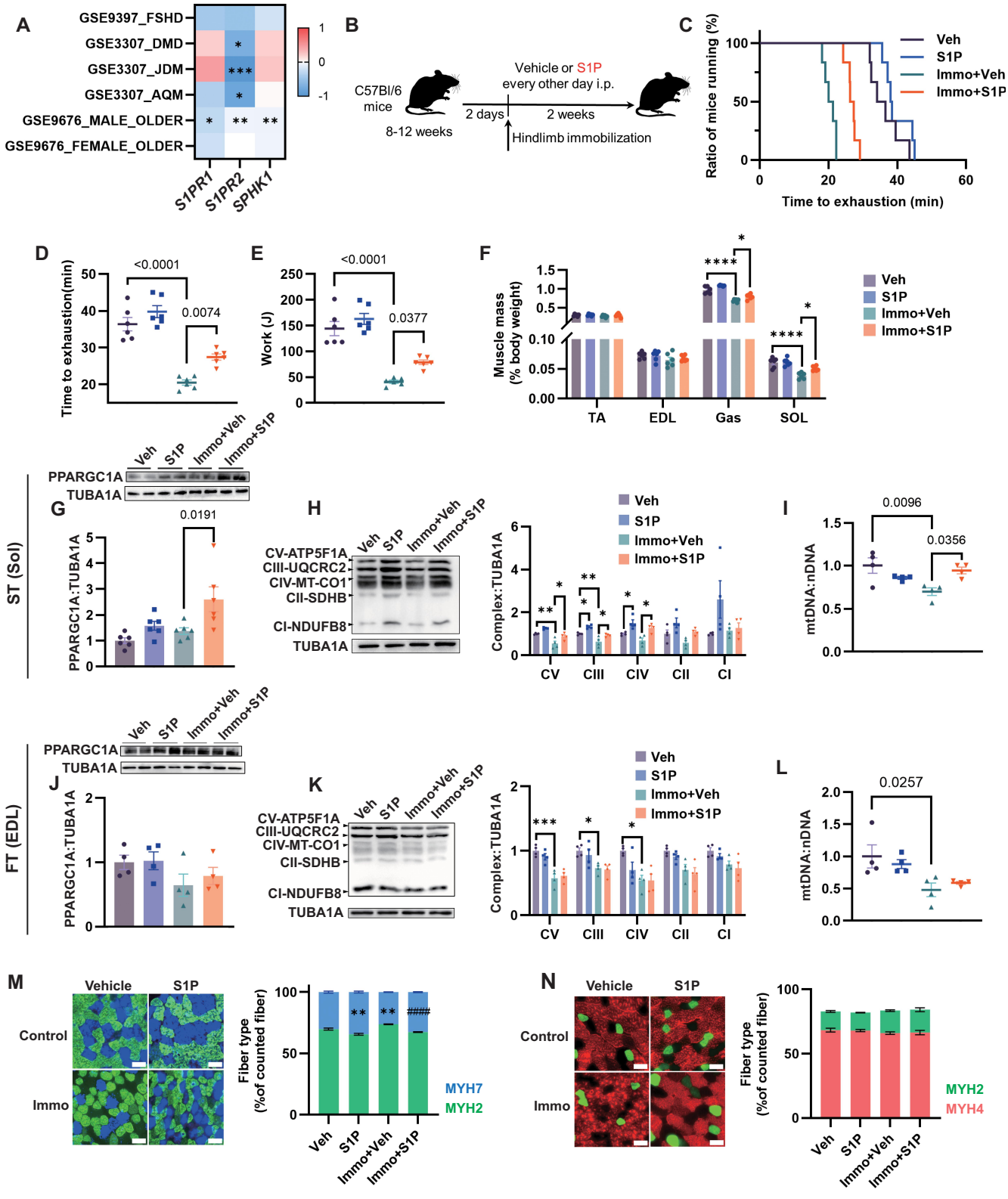

Figure 6. S1P improves slow-twitch muscle mitochondrial biogenesis and endurance performance in disuse atrophy mice. (A) Heatmap plot of transcriptomic datasets from humans suffering from muscle diseases and aging showing the relative expression of S1P signaling-related genes. The cell color represents $\log_2$ fold change. Adjusted *p* values are indicated as follows: *adjusted $p < 0.05$; **adjusted $p < 0.01$; ***adjusted $p < 0.001$ based on two-tailed student's t tests corrected for multiple testing using FDR. (B-N) 8-week-old male C57BL/6J mice were subjected to hindlimb immobilization and treated with intraperitoneal injections of vehicle (4 mg/mL BSA in normal saline) or S1P (1 mg/kg, every other day) for 2 weeks. (B) Experimental scheme. (C-E) running population (C), running time (D) and work (E) performed until exhaustion during treadmill stress test. (F) Muscle weight of control and immobilized mice treated with vehicle or S1P (n = 6). (G) protein levels of PPARGC1A in slow-twitch muscles (sol) (n = 6). (H) Protein levels of OXPHOS complexes in slow-twitch muscles (sol) (n = 4). (I) Ratios of mtDNA:nDNA measured by qPCR in slow-twitch muscles (sol) (n = 4). (J) Protein levels of PPARGC1A in fast-twitch muscles (EDL) (n = 4). (K) protein levels of OXPHOS complexes in fast-twitch muscles (EDL) (n = 4). (L) Ratios of mtDNA:nDNA measured by qPCR in fast-twitch muscles (EDL) (n = 4). (M) Representative images and quantification of fiber type staining of the slow-twitch muscles (sol) (n = 4). Blue, MYH7 (type I); green, MYH2 (type IIa). Scale bar: 50 μm. *p* values are indicated as follows: **$p < 0.01$ vs vehicle group. ###$p < 0.001$ vs Immobilized+Vehicle group. (N) Representative images and quantification of fiber type staining of the fast-twitch muscles (EDL) (n = 4). Green, MYH2 (type IIa); red, MYH4 (type IIb). Scale bar: 50 μm. All data are shown as the means ± SEM. Differences for more than two groups were assessed using one-way ANOVA with Tukey's post hoc test. *p* values are indicated as follows: *$p < 0.05$, **$p < 0.01$. ***$p < 0.001$, ****$p < 0.0001$.

mediated signaling was significantly downregulated in the liver and brain [49].

The present study found that the increased S1P by mitophagic degradation of ceramides activates mitochondrial adaptation through S1PR1/S1PR2 in slow-twitch muscles during endurance exercise. Injection of S1P caused mitochondrial biogenesis specifically in slow-twitch muscles, while pharmacological inhibition and genetic knockdown of S1PR1/S1PR2 blocked the mitochondrial adaptation in response to endurance exercise. Previous study in Hep G2 cells showed that exogenous S1P activated S1PR2-PRKA/PKA-CREB-PPARGC1A signaling cascades to promote mitochondrial biogenesis, but another study showed that endogenous S1P produced by SPHK2 regulated mitochondrial function through the interaction with prohibition 2 in the inner mitochondrial membrane, suggesting a S1PR-independent effect [50,51]. Further studies are required to determine whether exercise-induced S1P also interacts with mitochondrial proteins to regulate mitochondrial adaptation in response to endurance exercise.

Metabolic and functional disturbances in slow and fast-twitch myofibers play a complex role in the pathogenesis of muscle diseases [12,13]. Through the analysis of publicly available transcriptome data, this study identified reduced expression levels of *SPHK1* and *S1PR1/S1PR2* in muscle tissues from patients with muscle disorders and from aging males but not aging females. These findings suggest that the SPHK1-S1P-S1PR1/S1PR2 signaling pathway may play a more significant role in the muscle pathogenesis of males compared to females. However, to minimize variability associated with hormonal cycles, this study focused on male mice. Future studies including both sexes are needed to further validate and expand upon these findings. Notably, patients with inactivity-induced muscle atrophy and sarcopenia display more pronounced mitochondrial defects and reduced fatigue resistance in type I fibers compared to type II fibers [14,52]. Since SPHK1 and S1PR1/S1PR2 are highly expressed in type I muscle fibers, we hypothesize that S1P treatment may specifically mitigate mitochondrial defects associated with muscle atrophy, particularly in type I fibers. Actually, S1P largely improved the exercise capacity with increased mitochondrial adaptive responses in slow-twitch muscles in atrophy mice with hindlimb immobilization. Moreover, S1P increased the proportion of type I fibers in slow-twitch skeletal muscles from muscle atrophy mice. These findings align with previous studies demonstrating that increased S1P improves energy metabolism and muscle regeneration in the mdx mouse model of DMD [35,53,54], suggesting that pharmacologically targeting S1P signals emerge as a potential therapeutic strategy for individuals who are unable to engage in regular physical activity or for patients with muscle atrophy and dysfunctional diseases.

To summarize, our results emphasize the critical metabolic role of mitophagy in precisely regulating the ceramide-S1P balance to coordinate adaptive responses in skeletal muscles during exercise. The differential expression of the SPHK1-S1P-S1PR1/S1PR2 axis in slow-twitch and fast-twitch myofibers plays a key role in shaping the distinct activation patterns of mitophagy-S1P signaling in various muscle types. S1P treatment has been shown to enhance mitochondrial adaptive responses and exercise capacity in muscle-atrophy mice, particularly in slow-twitch muscles. These findings provide valuable insights into the metabolic distinctions between fast-twitch and slow-twitch myofibers and offer promise for the development of innovative therapeutic strategies for muscle dysfunction.

Materials and methods

Animal studies

All mice were housed in controlled facilities with a 12 h light/12 h dark cycle at 23 ± 3°C and food and water ad libitum. Male mice (C57BL/6J background, 8–12 weeks of age) were purchased from Peking University Health Science Center Laboratory Animal Center and used to avoid the effects of estrogen fluctuations on physiological responses and exercise performance. *fundc1* KO mice and mt-Keima mice inbred on a C57BL/6J background were generated as previously described [55]. To study the function of S1P, adult male mice were randomly divided into vehicle and S1P groups. Mice were administered vehicle (4 mg/mL BSA [Beyotime, ST025] in normal saline) or S1P (Sigma-Aldrich, S9666; 1 mg/kg, dissolved in vehicle) intraperitoneally every other day for four weeks for the treadmill stress test and further molecular assays. All animal studies were approved by the Institutional Animal Care and Use Committee of the Peking University Health Science Center (approval number: LA2020347).

Treadmill stress test and exercise protocol

Mice were acclimated to the treadmill for three days before the treadmill stress test. The acclimation process started at a speed of 8 m/min for 5 min on the first day, followed by 2 min at 10 m/min. On the second day, the speed was increased to 10 m/min for 5 min, followed by 2 min at 12 m/min. Afterward, the mice were given a day of rest. On the day of the study, the treadmill stress test was conducted at a 10° inclination with an initial speed of 10 m/min for 5 min. The treadmill speed was increased in 2 m/min increments every 3 min. Exhaustion was defined as the mice spending more than 10 s on the electric shocker.

In the case of acute exercise, adult male mice (8–12 weeks old) were randomly assigned to sedentary, exercised, and recovery (3 h post-exercise) groups. After a 3-day acclimation period, mice in the exercised and recovery groups were subjected to 60 min of moderate-intensity treadmill running at a 10° inclination and a speed of 15 m/min. Mice were euthanized immediately (for the exercised group) or 3 h after treadmill exercise (for the recovery group) using isoflurane anesthetization followed by cervical dislocation, and muscle tissues were collected and snap-frozen using liquid nitrogen.

Under the chronic exercise regimen, 8-week-old *fundc1* KO and WT mice underwent treadmill training for 6 weeks. The training protocol consisted of running at speeds of 15 m/min for 60 min, 4 days a week. WT mice were randomly divided into four groups during treadmill training: Mice

received intraperitoneal administration of vehicle (0.1% DMSO in normal saline) every other day. Mice were given W146 (MCE, HY-101395A) at a dose of 5 mg/kg every other day. Mice were administered with JTE-013 (MCE, HY-100675) at a dose of 5 mg/kg every other day. Mice were treated with CAY10444 (MCE, HY-119401) at a dose of 5 mg/kg every other day. Mice were euthanized three days after the last treadmill running session, and muscle tissues were harvested and snap-frozen using liquid nitrogen.

Isolation of mouse single myofibers

Isolation of single myofibers for type I and IIb was carried out from Sol and EDL muscles through enzymatic dissociation, following previously described methods [47]. In summary, the dissected muscles were digested with 2 mg/mL collagenase (Sigma-Aldrich, C0130) in DMEM (Macgene, CM15019) at 37°C for 60 min (for EDL) and 90 min (for Sol). Subsequently, the fibers were dissociated by gently pipetting the muscles up and down in DMEM. Each myofiber was then divided into two parts under a stereo microscope. One part of the myofiber was immediately lysed in lysis buffer prepared in accordance with the manufacturer's instructions (SMART-Seq HT kit, Takara, R400748) for sequencing, while the remaining part was solubilized in 1× protein loading buffer for 10 min at 100°C for MYH isoform identification. The MYH isoforms were separated by SDS-PAGE at 4°C for 12.5 h on 4% stacking (4% polyacrylamide 49:1, 30% glycerol, 70 mm Tris, pH 6.8, 4 mm EDTA and 0.4% SDS) and 8% separating gels (8% polyacrylamide 49:1, 30% glycerol, 200 mm Tris, pH 8.8, 100 mm glycine and 0.4% SDS). After silver staining (Fast Silver Stain Kit; Beyotime, P0017S), the bands corresponding to the MYH isoforms were identified via comparison with the MYH standard, which comprises lysates from the Sol and EDL muscles.

Hindlimb immobilization model

Male mice aged 8–12 weeks underwent hindlimb immobilization following a previously described protocol [56]. In brief, the mice were anesthetized with isoflurane and placed in the supine position. Their bilateral ankle joints were secured in a plantar flexed position, and a vinyl-coated steel wire (2.5 mm in diameter) was wrapped around the hip joints and bilateral hindlimbs to immobilize the hindlimbs at a right angle to the trunk. The immobilized mice were randomly divided into two groups: one group received vehicle, while the other group received S1P at a dose of 1 mg/kg every other day. After two weeks, the immobilization devices were removed, and the mice underwent a treadmill stress test.

Intramuscular AAV9 delivery of shRNA

shRNAs targeting *Sphk1*, *S1pr1*, or *S1pr2* were integrated into AAV9 vectors under the control of the U6 promoter and coupled with GFP. Control mice received a similar construct containing a scrambled peptide sequence. 1×10^{11} vg AAV9 particles were administered via intramuscular injections into the bilateral gastrocnemius muscles of mice. Two weeks post-injection, the mice underwent a six-week treadmill training regimen at a speed of 15 m/min. Mice were euthanized three days after the final treadmill session, and muscle tissues were harvested and snap-frozen in liquid nitrogen.

shRNA target sequence:
Sphk1: 5'-GCAGGTGACTAATGAAGACCT-3'
S1pr1: 5'-CCATGTAAACTGGGTCAAGTT-3'
S1pr2: 5'-GCCATCGTGGTGGAGAATCTT-3'

Isolation of human single myofibers

Human skeletal muscle tissues were collected as a by-product of internal fixation surgeries from tibia fracture patients at the Peking University People's Hospital as approved by the Ethics Committee of Peking University People's Hospital (ethics protocol: 2022PHB139–001). Muscle tissue samples (approximately 5 mm in length) were initially placed into 1 mL of RNAlater and stored at 4°C overnight and transferred to −20°C until isolation of muscle fibers. For each patient, around 200 myofibers were mechanically isolated under a stereoscope using fine tweezers at room temperature. Each myofiber was then segmented into two parts. Approximately one-third of each myofiber was solubilized in 1 × protein loading buffer at 100°C for 10 min to identify MYH isoforms via SDS-PAGE. The remaining portion was placed in 50 μL of TRIzol and stored at −80°C until MYH isoform identification. Myofibers with the same MYH isoform were pooled for RNA extraction.

Primary human muscle cells isolation and culture

Primary human myoblasts were isolated from human hindlimb muscle tissues as previously described [57]. Muscles were minced into small pieces within a few drops of HBSS and digested in 10 mL enzyme mix (5 mg/mL collagenase D [Roche 11,088,866,001] and 1.2 U/mL dispase II [Roche 04,942,078,001]) at 37°C for 1 h. Primary cells were then pelleted at 1100 g for 5 min and resuspended in DMEM with 20% fetal bovine serum (FBS; Hyclone, SH30396.03). Myoblasts were purified following fluorescence-activated cell sorting/FACS sorting using CD56 antibody (BioLegend 318,310) and plated on 0.1% gelatin (Aladdin, G274269)-coated plates. For maintenance and passaging, human myoblasts were cultured in DMEM supplemented with 20% FBS and 1% penicillin-streptomycin at 37°C with 5% CO_2. When the cells reached 80% confluence, they were transferred to differentiation medium consisting of DMEM and 2% horse serum (Thermo Fisher Scientific 16,050,122) for seven days until they differentiated into myotubes.

Cell culture and treatment of C2C12 mouse myoblast cell line

The C2C12 mouse myoblast cell line was purchased from Zomanbio (ZKC2006–1). All cells were authenticated by short tandem repeat/STR DNA profiling. C2C12 myoblasts were cultured in DMEM supplemented with 10% FBS and 1% penicillin-streptomycin at 37°C with 5% CO_2. For myogenesis differentiation, C2C12 myoblasts were transferred to DMEM

supplemented with 2% horse serum. Differentiated C2C12 myotubes were treated with 10 μM FCCP (MCE, HY-100410) for 4 h after pretreatment with 50 μM CQ (Sigma-Aldrich, C6628) for 4 h, 50 μM NOE (MCE, HY-107542) for 24 h or 5 μM SKI-II (MCE, HY-13822) for 24 h. Then, the FCCP was removed, and the cells were incubated with 10 μM S1P, 5 μM W146, 10 μM JTE-013 or 10 μM CAY10444 for 48 h.

siRNA transfection

Differentiated C2C12 myotubes were transfected with 10 nM siRNA targeting mouse *S1pr1*, *S1pr2*, *S1pr3*, *Sphk1*, or *Sphk2* or with a negative control agent in Opti-MEM (Thermo Fisher Scientific 31,985,070) with Lipofectamine RNAiMAX (Invitrogen 13,778,075). The media was exchanged for differential media 24 h post-transfection for pharmacological treatment.

siRNA sequence:

si*NC*, forward UUCUCCGAACGUGUCACGUTT and reverse ACGUGACACGUUCGGAGAATT;

si*Sphk1*, forward GAGGCAGAGAUAACCUUUATT and reverse UAAAGGUUAUCUCUGCCUCTT;

si*S1pr1*, forward AACUGACUUCAGUGGUGUUCATT and reverse UGAACACCACUGAAGUCAGUUTT;

si*S1pr2*, forward UUCUCCGAACGUGUCACGUTT and reverse ACGUGACACGUUCGGAGAATT;

Mitochondrial respirometry analysis

Mitochondrial respiration rates were measured in human myotubes and C2C12 mouse myotubes by Oxygraph 2K (Oroboros Inc., Innsbruck, Austria). In brief, cells were digested by trypsin and counted. Measurement of oxygen consumption in 10^6 cells were performed in DMEM. Following measurement of basal mitochondrial respiration, oligomycin (1 μg/mL; GlpBio, GC16533) was added to evaluate the uncoupled respiration; this was followed by the addition of the uncoupler FCCP (1 μM) to assess the maximal mitochondrial respiration, and then the addition of rotenone (0.5 μM; Sigma-Aldrich, R8875) and antimycin A (2.5 μM; GlpBio, GC49360) (R/AA). Respiration rates were expressed as "pmoles O_2/s/million cells".

Mt-Keima fluorescence imaging in vivo

Mice were anesthetized with isoflurane (3% for induction and 1% for maintenance) and maintained in the prone position. A 1–1.5 cm incision was made on the dorsal skin of the unilateral hindlimb to expose the gastrocnemius. The sponges were taped to both sides of the hindlimb to stabilize the tissue. Gastrocnemius fluorescence was imaged in two channels via two sequential excitations (488 nm, green; 552 nm, red) and with a 570–695 nm emission filter by using an SP8 Deep In Vivo Explorer (DIVE) microsystem (Leica). The two-photon excitation spectrum was detected with a multiphoton excitation laser with a wavelength ranging between 800 and 1256 nm. The two-photon excitation wavelength was identified to peak at ~900 nm and ~1100 nm, corresponding to the one-photon wavelength peaks (at 440 nm at neutral pH and 586 nm at acidic pH) [43]. Thus, the area under the curve was calculated to be between 800 and 1000 nm for neutral mitochondria and between 1000 and 1200 nm for mitochondria in lysosomes.

Immunofluorescence

C2C12 myotubes cultured on confocal dishes were stained with 500 nM MitoTracker™ Deep Red FM (Invitrogen, M22426) at 37°C for 30 min. After three washes with PBS (Macgene, CC008), the cells were fixed with 4% paraformaldehyde for 10 min. They were then permeabilized using 0.1% Triton X-100 (Applygen, A1009) in PBS for 30 min. To block nonspecific binding, the cells were treated with PBS containing 5% bovine serum albumin (BSA) at room temperature for 30 min. Subsequently, the cells were incubated overnight at 4°C with specific primary antibodies: mouse anti-ceramide IgM (Enzo Life Sciences, ALX-804-196-T050; 1:20) and rabbit anti-LC3 IgG (Cell Signaling Technology, 12741S; 1:100) in PBS with 1% BSA. Following three washes, the cells were incubated with secondary antibodies: Alexa Fluor 555 goat anti-rabbit IgG (Thermo Fisher Scientific, A-21429; 1:200) and Alexa Fluor 488 goat anti-mouse IgG (Thermo Fisher Scientific, A-21202; 1:200) for 1 h at room temperature. To visualize the cell nuclei, 4,6-diamidino-2-phenylindole (DAPI) staining was performed for 10 min. The resulting images were captured using confocal laser scanning microscopy (STED, Leica).

For immunostaining of muscle tissues, 8-μm cryosections of human and mouse muscle tissues were used in the procedure. The sections were blocked with 1% BSA in PBS and incubated with primary antibodies against MYH7 (DSHB, BA-D5; 1:10), MYH2 (DSHB, SC-71; 1:20), MYH4 (DSHB, BF-F3; 1:20), S1PR1 (Proteintech 55,133–1-AP; 1: 200), S1PR2 (Proteintech 21,180–1-AP; 1: 100) and SPHK1 (Proteintech 10,670–1-AP; 1: 100) at 4°C overnight. After washing, the sections were incubated with secondary antibodies against FITC-conjugated goat anti-mouse IgG1 (Jackson Laboratory, 115-095-205; 1:100), Violet 421-conjugated goat anti-mouse IgG2b (Jackson Laboratory, 115-675-207; 1:100), RRX-conjugated goat anti-mouse IgM (Jackson Laboratory, 115-295-020; 1:100) and Alexa Fluor 555 goat anti-rabbit IgG (Thermo Fisher Scientific, A-21429; 1:200) for 1 h at room temperature. The sections were imaged with an EVOS FL autoimaging system (Thermo Fisher Scientific).

Untargeted metabolomic analysis

100 mg gastrocnemius muscle was homogenized with 1 mL of a cold methanol: acetonitrile: water (2: 2: 1) solution and vortexed for 30 s. Samples were then sonicated for 1 min on ice and incubated at −20°C for 4 h, followed by 15 min centrifugation at 13,500 g and 4°C. The supernatants were collected and evaporated to dryness in a vacuum concentrator. The dry extracts were then dissolved in 100 μL of acetonitrile: water (1:1), sonicated for 5 min, vortexed for 30 s and centrifuged 5 min at 13,500 g and 4°C. The supernatants

were transferred to HPLC vials for subsequent LC/MS analysis.

All extracted samples were analyzed by ExionLC AD System (AB SCIEX) coupled with Triple TOF 6600+ (AB SCIEX). The separation was performed using a Waters Acquity HSS T3 column (1.8 µm, 2.1 × 100 mm) with the mobile phases containing water with 0.1% formic acid (phase A) and acetonitrile (phase B). The metabolites were separated at 0.3 mL/min using the following gradient conditions: 1% B at 0 min, 10% B at 2 min, 55% B at 6 min, 100% B at 15 min, 1% B at 16 min and 1% B at 20 min. The mass spectrometer was operated in positive and negative ionization modes with MS precursor ion scanning from 160 to 1200 Da and MS/MS product ion scanning from 50 to 1200 Da. Peak extraction were performed using XCMSplus (AB SCIEX) and metabolites were identified using MetDNA2 (http://metdna.zhulab.cn/). Differential metabolite analysis and pathway enrichment analysis were carried out using MetaboAnalyst5.0 (http://www.metaboanalyst.ca).

Mitochondrial isolation

Mitochondria were isolated through ultracentrifugation [58] with modifications using the mitochondrial isolation buffer (MIB): 225 mm mannitol (Aladdin, M108829), 75 mm sucrose (Aladdin, S112228), 10 mm HEPES, 1 mm EGTA, pH 7.4. Gastrocnemius muscles were minced in 1 mL of MIB with 0.5% BSA on ice and were subjected to incubation in MIB with 0.3 mg/mL of trypsin (Gibco 27,250–018) for 5 min at room temperature. Subsequently, the tissues were transferred to ice and diluted in 10 volumes of MIB with a protease inhibitor cocktail (Roche 04,693,116,001) and 0.5% BSA to halt trypsinization. After homogenization with ten strokes, the homogenates were centrifuged at 600 g for 10 min at 4°C. The supernatants were collected and then subjected to centrifugation at 600 g for 10 min at 4°C again to further sediment the unbroken cells and nuclei. The collected supernatants were centrifuged at 9000 g for 10 min at 4°C to precipitate the crude mitochondria. Following two washes with MIB, the crude mitochondria were resuspended in 200 µL of MIB and then layered on a Percoll (Cytiva 17,089,101) gradient (30%) and centrifuged at 95,000 g for 30 min at 4°C. The upper layer containing the mitochondrial-associated membrane (MAM) was removed, and the lower layer containing mitochondria was cautiously collected and diluted tenfold with MIB. The collected fraction was centrifuged at 6,300 g for 10 min at 4°C to pellet the purified mitochondria. After washing with MIB, the mitochondria pellets were stored at −80°C for western blot and metabolite analyses.

For cell samples, C2C12 myotubes were washed twice with PBS and scraped in 1 mL of MIB supplemented with 0.5% BSA. After homogenization by ten strokes, the cell suspensions were centrifuged at 600 × g for 10 min at 4°C. The rest of the procedure was the same as that described for tissue samples.

Quantitative analysis of sphingolipids

For cell and mitochondria samples, 500 µg (by protein) of C2C12 cells harvested by scraping and 100 µg (by protein) of mitochondrial pellets were resuspended in 100 µL of water. For tissue samples, 40 mg of gastrocnemius muscles were homogenized with 400 µL of water. All samples were extracted using four times the volume of a cold solution of chloroform and methanol (2:1) with the addition of 5 pmol of sphingolipid internal standard mix (Avanti Polar Lipids, LM6005) for ceramide quantification analysis. After 1 min of vortexing, the samples were sonicated for 1 min and left to incubate at room temperature for 30 min. Subsequently, a 10-min centrifugation at 13,500 g and 4°C was performed. The lower organic phases were then evaporated and dissolved in 100 µL of a solution of isopropanol and acetonitrile (1:1) for subsequent LC/MS analysis. For the quantification analysis of sphingosine and S1P, a single-phase extraction method was utilized due to the potential variability in recovering sphingoid bases in the organic phase of a conventional lipid extraction [59]. In summary, 500 µg (by protein) of C2C12 cells resuspended in 100 µL of water and 40 mg of gastrocnemius muscles homogenized in 400 µL of water were extracted using three times the volume of cold methanol with the addition of 5 pmol of sphingolipid internal standard mix. After 30 s of vortexing, the samples were sonicated for 1 min and then centrifuged at 13,500 g and 4°C for 10 min. The collected supernatants were evaporated and dissolved in 100 µL of a solution of acetonitrile and water (1:1).

Samples underwent analysis through injection onto a Waters Acquity BEH C18 column (1.7 µm, 2.1 × 100 mm) utilizing the UltiMate 3000 system (Thermo Fisher Scientific) coupled with the 4000 QTRAP (AB SCIEX). The separation was performed at a flow rate of 0.3 mL/min using mobile phases comprised of acetonitrile and water (60:40) with 5 mm ammonium formate (phase A) and isopropanol and acetonitrile (90:10) with 5 mm ammonium formate (phase B). The gradient used was as follows: 40% B at 0 min, 70% B at 2 min, 100% B at 7 min, 40% B at 7.1 min, and 40% B at 10 min. Quantification of ceramides and sphingoid bases was conducted using MultiQuant2.1 (AB SCIEX), and the sphingolipid abundance was normalized utilizing internal standards.

Smart-seq analysis

RNA extracted from single myofibers was reverse transcribed and amplified using a SMART-Seq HT kit. The cDNA was purified and size-selected with an AMPure XP system (Beckman Coulter, A63880) and quantified with a QuantiFluor dsDNA System (Promega, E2670). Sequencing libraries were created with a Nextera XT Kit (Illumina, FC-131–1024) using 1 ng of cDNA and purified with an AMPure XP system. The libraries were sequenced on a NovaSeq 6000 platform (Illumina), and paired-end 150 bp reads were generated. Sequenced reads were mapped to the mouse mm10 genome assembly using TopHat2. Differential expression analysis of the two groups and gene set enrichment analysis/GSEA were performed using DESeq2, clusterProfiler and aPEAR R package.

Bioinformatic analyses

Transcriptome datasets of single isolated mouse myofibers and human muscle disease specimens were retrieved from

the GEO database using the GEOquery R package. Expression data of human S1P signaling-related genes were obtained from 803 postmortem skeletal muscle biopsies available in the GTEx database [60]. Mouse S1P signaling-related genes and phenotypic traits from the BXD mouse genetic population [39] were obtained from GeneNetwork2 (www.genenetwork.org/). A gene expression dataset (EPFLMouseMuscleCD+HFDRMA1211) and phenotypic trait information (17738, 17742, 17750, 17758) were used for Pearson correlation analysis with R software.

Western blot

Muscle tissues, C2C12 cells and mitochondrial samples were lysed using RIPA lysis buffer (Thermo Fisher Scientific 89,900) with protease inhibitor cocktail (Roche 04,693,116,001), and the concentrations of the extracted proteins were measured with a Rapid Gold BCA Kit (Thermo Fisher Scientific, A53227). The proteins were resolved by SDS-PAGE and transferred to PVDF membranes (Merck Millipore, ISEQ00010). The membranes were blocked in TBST with 5% skim milk for 1 h and then incubated with primary antibodies against the following proteins: LC3A/B (Cell Signaling Technology, 12741S; 1:1000), TUBA1A/α-tubulin (Biodragon, B1052; 1: 5000), TIMM23 (Proteintech 67,535–1-I; 1: 5000), PPARGC1A/PGC-1α (Proteintech 66,369–1-Ig; 1: 3000), S1PR1 (Proteintech 55,133–1-AP; 1: 3000), S1PR2 (Proteintech 21,180–1-AP; 1: 600), S1PR3 (Abcam, ab108370; 1: 2000), SPHK1 (Proteintech 10,670–1-AP; 1: 1000) and OXPHOS (Abcam, ab110413; 1: 1000) at 4°C overnight. After three washes with TBST, the membranes were incubated with HRP-conjugated secondary antibodies. The protein bands on the membranes were visualized by chemiluminescence using a ChemiDoc XRS+ System (Bio-Rad, USA), and the band density was quantified using ImageJ.

Quantitative PCR (qPCR) analysis

RNA was extracted from muscle tissues using TRIzol (Invitrogen 15,596,026). The mRNA was reverse transcribed to cDNA using All-In-One 5X RT MasterMix (Applied Biological Materials, G490). Real-time qPCR was performed using SYBR green fluorescence (GenStar, A301). The CT values of *S1pr1*, *S1pr2*, *S1pr3*, *Sphk1* and *Sphk2* were normalized to the corresponding CT values of *Actb/β-actin* to calculate the relative expression levels of these genes. Genomic DNA and mitochondrial DNA were extracted using a genomic DNA extraction kit (Tiangen Biotech, DP304). mtDNA levels were quantified by the relative amount ratio of mtDNA determined by the *mt-Rnr1/12S* ribosomal RNA gene to nucleic DNA determined by *Lpl* in mice, while mtDNA levels in human samples were quantified by the ratio of *MT-ND1* to *B2M*. The mitochondrial turnover ratio was determined by subtracting the mtDNA level at 0 h following FCCP stimulation from the mtDNA level at 48 h poststimulation and then normalizing the value to the mtDNA level at 0 h after FCCP stimulation.

Primers for q-PCR:

Human MT-ND1, forward CCCTAAAACCCGCCACATCT and reverse GAGCGATGGTGAGAGCTAAGGT;

Human B2M, forward CCAGCAGAGAATGGAAAGTCAA and reverse TCTCTCTCCATTCTTCAGTAAGTCAACT;

Human SPHK1, forward GCTGGCAGCTTCCTTGAACCAT and reverse GTGTGCAGAGACAGCAGGTTCA;

Human S1PR1, forward CCTGTGACATCCTCTTCAGAGC and reverse CACTTGCAGCAGGACATGATCC;

Human S1PR2, forward TGGAAACGCAGGAGACGACCTC and reverse CGAGTGGAACTTGCTGTTTCGG;

Human ACTB, forward CACCATTGGCAATGAGCGGTTC and reverse AGGTCTTTGCGGATGTCCACGT;

Mouse mt-Rnr1/12S RNA, forward CTCAAAGGACTTGGCGGTAC and reverse TTCCCATTTCATTGGCTACAC;

Mouse Lpl, forward GGATGGACGGTAAGAGTGATTC and reverse ATCCAGGGTAGCAGACAGGT;

Mouse S1pr1: forward ACTTTGCGAGTGAGCTG and reverse AGTGAGCCTTCAGTTACAGC;

Mouse S1pr2: forward, TTCTGGAGGGTAACACAGTGGT; reverse, ACACCCTTTGTATCAAGTGGCA;

Mouse S1pr3: forward, TGGTGTGCGGCTGTCTAGTCAA; reverse, CACAGCAAGCAGACCTCCAGA;

Mouse Sphk1: forward, TGTCACCCATGAACCTGCTGTCCCTGCACA; reverse, AGAAGGCACTGGCTCCAGAGGAACAAG;

Mouse Sphk2: forward, ACAGAACCATGC CCGTGAG; reverse, AGGTCAACACCGACAACCTG;

Mouse Actb: forward, GGCTGTATT CCCCTCCATCG; reverse, CCAGTTGGTAACAATGCCATGT.

Quantification and statistical analysis

All the data are presented as the mean ±SEM. Prism 9 (GraphPad) and R were used for statistical analysis and generation of figures. The normality of the distribution of the data was determined by the Shapiro–Wilk normality test. For normally distributed data, unpaired Student's t test and one-way ANOVA with Tukey's post hoc analysis were used to compare differences between two groups and multiple groups, respectively. Non-normally distributed data were analyzed by the Mann–Whitney U test for two groups or the Kruskal–Wallis test for multiple groups. $p < 0.05$ was considered to indicate statistical significance. The exact n number for each experiment is provided in the respective figure legend.

Disclosure statement

No potential conflict of interest was reported by the author(s).

Funding

This work was supported by grants from the National Key Research and Development Program of China [2020YFA0803802], the National Natural Science Foundation of China [32371242, 91954117, 82000348] and the Beijing Municipal Natural Science Foundation grant 7222193.

Data availability statement

The untargeted metabolomics dataset is available as table S1. The RNA-seq data has been deposited in NCBI's Gene Expression Omnibus and are accessible through GEO: GSE244547. Any additional information reported in this paper is available from the corresponding author.

References

[1] Koch LG, Kemi OJ, Qi N, et al. Intrinsic aerobic capacity sets a divide for aging and longevity. Circ Res. 2011;109 (10):1162–1172. doi: 10.1161/CIRCRESAHA.111.253807

[2] Blair SN. Physical inactivity: the biggest public health problem of the 21st century. Br J Sports Med. 2009;43:1–2.

[3] Ekelund LG, Haskell WL, Johnson JL, Whaley FS, Criqui MH, Sheps DS. Physical fitness as a predictor of cardiovascular mortality in asymptomatic North American men. The lipid research clinics mortality follow-up study. N Engl J Med. 1988;319 (21):1379–1384. doi: 10.1056/NEJM198811243192104

[4] Gulati M, Pandey DK, Arnsdorf MF, et al. Exercise capacity and the risk of death in women: the st james women take heart project. Circulation. 2003;108(13):1554–1559. doi: 10.1161/01.CIR.0000091080.57509.E9

[5] Myers J, Prakash M, Froelicher V, et al. Exercise capacity and mortality among men referred for exercise testing. N Engl J Med. 2002;346(11):793–801. doi: 10.1056/NEJMoa011858

[6] Liu J, Liang X, Zhou D, et al. Coupling of mitochondrial function and skeletal muscle fiber type by a miR-499/Fnip1/AMPK circuit. EMBO Mol Med. 2016;8(10):1212–1228. doi: 10.15252/emmm.201606372

[7] Vainshtein A, Hood DA. The regulation of autophagy during exercise in skeletal muscle. J Appl Physiol. 2016;120(6):664–673. doi: 10.1152/japplphysiol.00550.2015

[8] Egan B, Zierath JR. Exercise metabolism and the molecular regulation of skeletal muscle adaptation. Cell Metab. 2013;17 (2):162–184. doi: 10.1016/j.cmet.2012.12.012

[9] Deshmukh AS, Steenberg DE, Hostrup M, et al. Deep muscle-proteomic analysis of freeze-dried human muscle biopsies reveals fiber type-specific adaptations to exercise training. Nat Commun. 2021;12(1):304. doi: 10.1038/s41467-020-20556-8

[10] Jeneson JAL, de Snoo MW, Verlinden NAT, et al. Treadmill but not wheel running improves fatigue resistance of isolated extensor digitorum longus muscle in mice. Acta Physiol (Oxf). 2007;190 (2):151–161. doi: 10.1111/j.1748-1716.2007.01680.x

[11] Moro T, Brightwell CR, Volpi E, et al. Resistance exercise training promotes fiber type-specific myonuclear adaptations in older adults. J Appl Physiol (1985). 2020;128:795–804.

[12] Conley KE, Jubrias SA, Amara CE, et al. Mitochondrial dysfunction: impact on exercise performance and cellular aging. Exerc Sport Sci Rev. 2007;35(2):43–49. doi: 10.1249/JES.0b013e31803e88e9

[13] Handschin C, Kobayashi YM, Chin S, et al. PGC-1α regulates the neuromuscular junction program and ameliorates duchenne muscular dystrophy. Genes Dev. 2007;21(7):770–783. doi: 10.1101/gad.1525107

[14] Talbot J, Maves L. Skeletal muscle fiber type: using insights from muscle developmental biology to dissect targets for susceptibility and resistance to muscle disease. Wiley Interdiscip Rev Dev Biol. 2016;5(4):518–534. doi: 10.1002/wdev.230

[15] Laurila P-P, Wohlwend M, Imamura de Lima T, et al. Sphingolipids accumulate in aged muscle, and their reduction counteracts sarcopenia. Nat Aging. 2022;2(12):1159–1175. doi: 10.1038/s43587-022-00309-6

[16] Wohlwend M, Laurila P-P, Williams K, et al. The exercise-induced long noncoding RNA CYTOR promotes fast-twitch myogenesis in aging. Sci Transl Med. 2021;13(623): eabc7367. doi: 10.1126/scitranslmed.abc7367

[17] Rai M, Demontis F. Systemic nutrient and stress signaling via Myokines and myometabolites. Annu Rev Physiol. 2016;78 (1):85–107. doi: 10.1146/annurev-physiol-021115-105305

[18] Rai M, Demontis F, van Praag H, et al. Muscle-to-brain signaling via Myokines and myometabolites. Brain Plast. 2022;8(1):43–63. doi: 10.3233/BPL-210133

[19] Pang BPS, Chan WS, Chan CB. Mitochondria homeostasis and oxidant/antioxidant balance in skeletal muscle—do myokines play a role? Antioxidants (Basel). 2021;10(2):10. doi: 10.3390/antiox10020179

[20] Burtscher J, Soltany A, Visavadiya NP, et al. Mitochondrial stress and mitokines in aging. Aging Cell. 2023;22(2):e13770. doi: 10.1111/acel.13770

[21] Shirai T, Uemichi K, Hidaka Y, et al. Effect of lactate administration on mouse skeletal muscle under calorie restriction. Curr Res Physiol. 2021;4:202–208. doi: 10.1016/j.crphys.2021.09.001

[22] Hashimoto T, Hussien R, Oommen S, et al. Lactate sensitive transcription factor network in L6 cells: activation of MCT1 and mitochondrial biogenesis. Faseb J. 2007;21(10):2602–2612. doi: 10.1096/fj.07-8174com

[23] Yuan Y, Xu P, Jiang Q, et al. Exercise-induced α-ketoglutaric acid stimulates muscle hypertrophy and fat loss through OXGR1-dependent adrenal activation. Embo J. 2020;39:e103304.

[24] He C, Bassik MC, Moresi V, et al. Exercise-induced BCL2-regulated autophagy is required for muscle glucose homeostasis. Nature. 2012;481(7382):511–515. doi: 10.1038/nature10758

[25] Grumati P, Coletto L, Schiavinato A, et al. Physical exercise stimulates autophagy in normal skeletal muscles but is detrimental for collagen vi-deficient muscles. Autophagy. 2011;7 (12):1415–1423. doi: 10.4161/auto.7.12.17877

[26] Fritzen AM, Madsen AB, Kleinert M, et al. Regulation of autophagy in human skeletal muscle: effects of exercise, exercise training and insulin stimulation. J Physiol. 2016;594:745–761.

[27] Mucha O, Kaziród K, Podkalicka P, et al. Dysregulated autophagy and mitophagy in a mouse model of Duchenne muscular dystrophy remain unchanged following heme oxygenase-1 knockout. Int J Mol Sci. 2021;23(1):23. doi: 10.3390/ijms23010470

[28] Grumati P, Coletto L, Sabatelli P, et al. Autophagy is defective in collagen VI muscular dystrophies, and its reactivation rescues myofiber degeneration. Nat Med. 2010;16(11):1313–1320. doi: 10.1038/nm.2247

[29] Fu T, Xu Z, Liu L, et al. Mitophagy directs muscle-adipose crosstalk to alleviate dietary obesity. Cell Rep. 2018;23(5):1357–1372. doi: 10.1016/j.celrep.2018.03.127

[30] Rabinowitz JD, White E. Autophagy and metabolism. Science. 2010;330(6009):1344–1348. doi: 10.1126/science.1193497

[31] Ueda N. A rheostat of ceramide and sphingosine-1-phosphate as a determinant of oxidative stress-mediated kidney injury. Int J Mol Sci. 2022;23(7):23. doi: 10.3390/ijms23074010

[32] Newton J, Lima S, Maceyka M, et al. Revisiting the sphingolipid rheostat: evolving concepts in cancer therapy. Exp Cell Res. 2015;333(2):195–200. doi: 10.1016/j.yexcr.2015.02.025

[33] Cordeiro AV, Silva VRR, Pauli JR, et al. The role of sphingosine-1-phosphate in skeletal muscle: physiology, mechanisms, and clinical perspectives. J Cell Physiol. 2019;234 (7):10047–10059. doi: 10.1002/jcp.27870

[34] Zanin M, Germinario E, Dalla Libera L, et al. Trophic action of sphingosine 1-phosphate in denervated rat soleus muscle. Am J Physiol Cell Physiol. 2008;294(1):C36–C46. doi: 10.1152/ajpcell.00164.2007

[35] Ieronimakis N, Pantoja M, Hays AL, et al. Increased sphingosine-1-phosphate improves muscle regeneration in acutely injured mdx mice. Skelet Muscle. 2013;3(1):20. doi: 10.1186/2044-5040-3-20

[36] Danieli-Betto D, Germinario E, Esposito A, et al. Sphingosine 1-phosphate protects mouse extensor digitorum longus skeletal muscle during fatigue. Am J Physiol Cell Physiol. 2005;288: C1367–C73.

[37] Germinario E, Bondì M, Cencetti F, et al. S1P3 receptor influences key physiological properties of fast-twitch extensor digitorum longus muscle. J Appl Physiol (1985). 2016;120:1288–1300.
[38] Błachnio-Zabielska A, Baranowski M, Zabielski P, et al. Effect of exercise duration on the key pathways of ceramide metabolism in rat skeletal muscles. J Cell Biochem. 2008;105:776–784.
[39] Andreux PA, Williams EG, Koutnikova H, et al. Systems genetics of metabolism: the use of the BXD murine reference panel for multiscalar integration of traits. Cell. 2012;150(6):1287–1299. doi: 10.1016/j.cell.2012.08.012
[40] Dany M, Gencer S, Nganga R, et al. Targeting FLT3-ITD signaling mediates ceramide-dependent mitophagy and attenuates drug resistance in AML. Blood. 2016;128(15):1944–1958. doi: 10.1182/blood-2016-04-708750
[41] Thomas RJ, Oleinik N, Panneer Selvam S, et al. HPV/E7 induces chemotherapy-mediated tumor suppression by ceramide-dependent mitophagy. EMBO Mol Med. 2017;9(8):1030–1051. doi: 10.15252/emmm.201607088
[42] Dany M, Ogretmen B. Ceramide induced mitophagy and tumor suppression. Biochim Biophys Acta. 2015;1853(10):2834–2845. doi: 10.1016/j.bbamcr.2014.12.039
[43] Sun N, Malide D, Liu J, et al. A fluorescence-based imaging method to measure in vitro and in vivo mitophagy using mt-keima. Nat Protoc. 2017;12(8):1576–1587. doi: 10.1038/nprot.2017.060
[44] Sun N, Yun J, Liu J, et al. Measuring in vivo mitophagy. Mol Cell. 2015;60:685–696.
[45] Raz V, Riaz M, Tatum Z, et al. The distinct transcriptomes of slow and fast adult muscles are delineated by noncoding RNAs. Faseb J. 2018;32(3):1579–1590. doi: 10.1096/fj.201700861R
[46] Wu H, Gallardo T, Olson EN, et al. Transcriptional analysis of mouse skeletal myofiber diversity and adaptation to endurance exercise. J Muscle Res Cell Motil. 2003;24(8):587–592. doi: 10.1023/B:JURE.0000009968.60331.86
[47] Chemello F, Grespi F, Zulian A, et al. Transcripnd miR-142-3p as regulators of metabolism in skeletal muscle. Cell Rep. 2019;26(13):3784–3797.
[48] Flockhart M, Nilsson LC, Tais S, et al. Excessive exercise training causes mitochondrial functional impairment and decreases glucose tolerance in healthy volunteers. Cell Metab. 2021;33(5):957–970.
[49] Yambire KF, Fernandez-Mosquera L, Steinfeld R, et al. Mitochondrial biogenesis is transcriptionally repressed in lysosomal lipid storage diseases. Elife. 2019;8. doi: 10.7554/eLife.39598
[50] Shen Z, Liu C, Liu P, et al. Sphingosine 1-phosphate (S1P) promotes mitochondrial biogenesis in hep G2 cells by activating peroxisome proliferator-activated receptor γ coactivator 1α (PGC-1α). Cell Stress Chaperones. 2014;19:541–548.
[51] Strub GM, Paillard M, Liang J, et al. Sphingosine-1-phosphate produced by sphingosine kinase 2 in mitochondria interacts with prohibitin 2 to regulate complex IV assembly and respiration. Faseb J. 2011;25(2):600–612. doi: 10.1096/fj.10-167502
[52] Fukunaga T, Mori S, Omura T, et al. Muscle fiber type specific alterations of mitochondrial respiratory function and morphology in aged female mice. Biochem Biophys Res Commun. 2021;540:116–122. doi: 10.1016/j.bbrc.2020.11.071
[53] De la Garza-Rodea AS, Moore SA, Zamora-Pineda J, et al. Sphingosine phosphate lyase is upregulated in Duchenne muscular dystrophy, and its inhibition early in life attenuates inflammation and dystrophy in mdx mice. Int J Mol Sci. 2022;23(14):7579.
[54] Nguyen-Tran D-H, Hait NC, Sperber H, et al. Molecular mechanism of sphingosine-1-phosphate action in Duchenne muscular dystrophy. Dis Model Mech. 2014;7:41–54.
[55] Liu R, Xu C, Zhang W, et al. FUNDC1-mediated mitophagy and HIF1α activation drives pulmonary hypertension during hypoxia. Cell Death Dis. 2022;13(7):634. doi: 10.1038/s41419-022-05091-2
[56] Onda A, Kono H, Jiao Q, et al. New mouse model of skeletal muscle atrophy using spiral wire immobilization. Muscle Nerve. 2016;54(4):788–791. doi: 10.1002/mus.25202
[57] Spinazzola JM, Gussoni E. Isolation of primary human skeletal muscle cells. Bio Protoc. 2017;7(21). doi: 10.21769/BioProtoc.2591
[58] Wieckowski MR, Giorgi C, Lebiedzinska M, et al. Isolation of mitochondria-associated membranes and mitochondria from animal tissues and cells. Nat Protoc. 2009;4(11):1582–1590. doi: 10.1038/nprot.2009.151
[59] Shaner RL, Allegood JC, Park H, et al. Quantitative analysis of sphingolipids for lipidomics using triple quadrupole and quadrupole linear ion trap mass spectrometers. J Lipid Res. 2009;50:1692–1707.
[60] GTEx Consortium, Ardlie KG, Deluca DS. The Genotype-Tissue Expression (GTEx) pilot analysis: multitissue gene regulation in humans. Science. 2015;348(6235):648–660. doi: 10.1126/science.1262110